$69 \atop p.$

N64 10102

CODE-1

NASA CR 52201

R63SD29

MEASUREMENTS OF HYPERVELOCITY STAGNATION POINT HEAT TRANSFER IN SIMULATED PLANETARY ATMOSPHERES

J.S. GRUSZCZYNSKI
W.R. WARREN, JR.

SPACE SCIENCES LABORATORY

GENERAL ⚙ ELECTRIC

MISSILE AND SPACE DIVISION

SPACE SCIENCES LABORATORY

ELECTRON PHYSICS SECTION

MEASUREMENTS OF HYPERVELOCITY
STAGNATION POINT HEAT TRANSFER IN
SIMULATED PLANETARY ATMOSPHERES *

By

J. S. Gruszczynski
W. R. Warren

NASA CR-52201; R63SD29

March 1963

MISSILE AND SPACE DIVISION

GENERAL ⊕ ELECTRIC

Philadelphia, Pa.

GENERAL ⊕ ELECTRIC

SPACE SCIENCES LABORATORY
MISSILE AND SPACE DIVISION

TECHNICAL INFORMATION SERIES

AUTHOR	SUBJECT CLASSIFICATION	NO.
J. S. Gruszczynski W. R. Warren, Jr.		R63SD29
		DATE March, 1963
TITLE Measurements of Hypervelocity Stagnation Point Heat Transfer in Simulated Planetary Atmospheres		**G. E. CLASS** Class I
		GOV. CLASS Unclassified
REPRODUCIBLE COPY FILED AT MSD LIBRARY, DOCUMENTS LIBRARY UNIT, VALLEY FORGE SPACE TECHNOLOGY CENTER, KING OF PRUSSIA, PA.		**NO. PAGES** 65

SUMMARY

The heat transfer to the stagnation region of a hemi-spherical body at flight velocities up to 40,000 ft/sec in two CO_2-N_2 gas mixtures corresponding to the expected atmosphere of Venus has been investigated experimentally in the electrically driven hypervelocity shock tube. These results are compared with heat transfer data in pure CO_2 and pure N_2. Calculations of radiative heat transfer contribution to the total heating are shown. Also, shock tube performance in two gas compositions as used in these experiments was computed.

An attempt was made to measure radiant heat transfer to the stagnation region using the newly developed cavity gage.

By cutting out this rectangle and folding on the center line, the above information can be fitted into a standard card file.

AUTHOR _____

COUNTERSIGNED _____

CONTENTS

INTRODUCTION

One of the many problems connected with space flight is the intense heating experienced by the vehicle during its entry into the planetary atmosphere. During the flight at relatively low altitudes a shock wave forms ahead of the body. The free stream gas passes through this shock wave and undergoes a large increase in internal energy which is sufficient to cause dissociation of molecules and even partial ionization of the gas. This hot, chemically reacting gas flows around the vehicle and heat is transferred to its surface. Two modes of heat transfer can be distinguished. One is the aerodynamic heat transfer process which includes conduction, convection and diffusion of molecules, atoms, ions and electrons across the boundary layer; the other is the radiation from the hot gas cap (shock layer) surrounding the forward section of the vehicle.

The purpose of this experimental study was to investigate the aerodynamic heat transfer to the stagnation point of a blunt body in a hypersonic flow of simulated atmospheres of Venus. Besides supporting the available analytical studies, the results of this work provide heat transfer data for a range of flight conditions beyond the scope of the present analyses.

It can be shown that at the stagnation point of a blunt body in hypersonic flight the aerodynamic heating is accurately simulated if the conditions at the edge of the boundary layer including the pressure distribution and wall conditions are correctly reproduced.

The experiments were carried out in the newly developed arc-heated 2" shock tube which is capable of producing in the laboratory the environmental conditions encountered by the entry vehicle. The correct conditions of enthalpy and stagnation pressure were simulated in two assumed composition models of Venusian atmosphere for flight velocities up to about 40,000 ft/sec.

Preliminary analytical work involved the calculations of shock tube performance for both test gas mixtures corresponding to the specified atmosphere of Venus. Thermodynamic properties behind incident and normal shocks, and at the stagnation point of the hemispherical body were computed. An estimation of the radiation heat flux was also made to assess the magnitude of radiant heating sensed by the stagnation point heat gage. To confirm theoretical calculations an attempt has been made to measure the radiant heating using a new type of a total radiation gage. The primary objective of these radiation measurements was to demonstrate that the radiative contribution to the measured heating results was small, that is, they are used to verify that the measured heat transfer rates are essentially caused by the convective or boundary layer heat transfer mechanism.

TEST FACILITY

The shock tube has been used for many years in experiments for the generation of aerodynamic data in flows of high energy and high stagnation pressure (Refs. 1, 2, and 3). The demand for an experimental facility in the area of simulation of orbital or even super-orbital enthalpies and pressures forced further development of its performance. It was obvious that this was beyond the capability of a conventional combustion driven shock

- 2 -

tube. The arc-heated shock tube used for the present experiments was developed specifically for that purpose (Ref. 4). It was originally designed as a prototype of a large facility but has been used successfully in experimental investigations. Numerous heat transfer tests were run with air, CO_2 and N_2 as the test gas and some of the data were reported in Reference 4.

Figure 1 shows schematically the design details of the whole shock tube assembly. The driven section is 2 in. in diameter and it is 135.5 in. long. The driver is 17 in. inside length with 2 1/4 in. internal diameter. A Lexan cylindrical sleeve with 1/4 in. wall thickness fits inside the driver tube. It is used to provide electrical insulation along the arc path; that is, it insures that the arc discharge is contained within the driver gas and that the energy is uniformly distributed axially along the driver. A thin wire is used to initiate the arc discharge. This is located on axis so that the wall losses will be uniform in the axial direction.

The high voltage electrode which is insulated from the driver end flange by a Lexan bushing is in the form of a hollow copper cylinder with a 3/8 in. diameter. A 1/8 in. diameter brass rod insulated by teflon tubing and held in position by a tapered steel washer and a nut is inserted through the center of the main electrode. A 5 mil tungsten wire is attached to the spider electrode at the diaphragm end of the driver and by about 1 in. long cotton thread to the copper main electrode. The position of the brass rod relative to the main electrode determines the breakdown voltage. This adjustment is made with the main capacitors bank disconnected, using a small capacitor to prevent breaking of the wire.

- 3 -

The electrical circuit for the driver heating system is shown in Figure 2.a.   The energy for the arc discharge is stored in forty-seven capacitors, each rated at 5 microfarads and 20,000 volts.

Figure 2.b. shows a typical current wave form. It indicates that the circuit is critically damped and that the energy is completely dissipated in about 50 microseconds, and before the diaphragm opens which occurs about 150 microseconds later. Full description of the considerations entering into the design of this test facility is presented by Warren, et al (Ref. 4).

Helium is used as the gas heated in the driver. The diaphragm separating the driver and the driven section of the shock tube is made of stainless steel. It is scribed to a controlled depth (generally 20% - 40% of the thickness) along two diametrical cross lines. The required conditions of a given test run dictate the proper selection of the diaphragm. The diaphragm is found to open cleanly with a negligible loss of material.

As indicated in Ref. 4 , an extensive research program was necessary before a satisfactory operation of this facility was achieved. A photograph of the complete test facility including the power supply, vacuum pumps, etc., is shown in Figure 3.   The performance of the tube in air is shown in Figure 4 where the attainable shock velocity is plotted as a function of initial pressure and energy input. The experimental data indicate that shock velocity up to 30,000 ft/sec can be obtained with 1 mm Hg driven tube initial pressure and full energy in the capacitors. With a lower initial pressure, shock velocity up to 36,000 ft/sec can be reached. Superimposed is a curve depicting the performance of a combustion driver facility. The limitation of the latter is self-evident.

- 4 -

EXPERIMENTAL TECHNIQUE

Large amounts of carbon-like residue are normally found to cover the driver tube walls and models after each test. The origin of this is the Lexan sleeve used to insulate the driver. It appears that during the electrical discharge the inner wall surface of the sleeve decomposes slightly and particles of carbon so formed are carried along the driven tube by the expanding driver gas.

To insure a low degree of contamination of the test gas several steps were taken after each test run and before a new run was made. The driven tube was thoroughly wiped with alcohol until no trace of carbon could be noticed on the inner walls. The same applies to the test model, which was also carefully cleaned, and the gage surface brought to approximately the same degree of reflectivity as in the previous run. The tube was then evacuated down to about 10 - 20 microns pressure. The leak rate was then measured. If the rate did not exceed 10 microns per minute, the tube was considered to be in satisfactory condition.

Next the tube was filled with the test gas to the required test pressure P_1 (normally either 1 mm or 5 mm Hg). To further minimize the contamination of the test gas by impurities due to outgassing of the walls, the test gas mixture was allowed to flow through the tube at a rate of approximately 20 tube volumes per minute for about 20 - 30 minutes. The initial pressure in the driven tube was measured with a McLeod gage.

The driven section of the 2" shock tube is equipped with six port

- 5 -

holes equally spaced at 11" apart as shown in Figure 5. The model nor-
mally is located about 1/8 in. behind position 6. The signal from the piezo-
electric pressure gage located at position 1 was used to trigger the scopes
displaying heat transfer gage output.

Shock velocity was monitored by measuring the elapsed time for the
incident shock wave to travel between positions 3-5, 4-5 and 5-6. Pressure
gages were used as time of arrival sensors. The last two intervals were
used to determine the shock velocity for the particular test run. The scatter
between data for these two intervals is invariably within the reading accur-
acy of the wave transit time for one interval ($\pm$ 1-1/2%). This indicates the
existence of only small incident shock wave attenuation effects (if any). A
two color pyrometer was used to monitor the luminosity behind the incident
shock wave. The violet range extended between 3500 - 4500 $\overset{o}{A}$, while the
red region response was between 6000 - 8000 $\overset{o}{A}$. The history of the pressure
behind the incident shock wave was also observed by displaying the output
of a pressure gage from position 5. The output was filtered to eliminate the
ringing of the gage whose natural frequency lies around 40 kc.

The heat transfer rate was determined with a calorimeter gage
mounted at the stagnation point of the hemispherical model 1/2 in. in diam-
eter (Figure 6). The design dimensions of the gage were 1/16 in. wide by
3/16 in. long. The gage element itself was made of 0.004 in. thick Hytemco
(iron-nickel) alloy. The leads were brought out from the gage through the
internal cavity of the model and its supporting sting and were connected in

- 6 -

a circuit shown schematically in Figure 7. One of the features (Ref. 4) of the circuit is the grounding of the instrument circuit in common with the driver circuit and the connection of the gage leads across a balanced differential amplifier. These steps allow extraneous electrical effects observed earlier in the experiments to be reduced to a level such that they do not preclude the observation of the heat transfer signal.

The output of the heat transfer gage was displayed and photographed on four oscilloscopes in parallel, each with a different sweep rate. The rates were 20, 10, 5 and 2 μsec/cm. Since the region of interest (corresponding to the steady flow conditions) lies approximately within the first 20 μ sec from the moment of the bow shock formation, either the five or two μsec/cm records were used to read off the heat transfer rate.

The relation between the heat rate and the change of the voltage with time across the gage is expressed by the simple expression

$$\dot{q} = K \frac{1}{E_o} \frac{dE}{dt}$$

and

$$K = \frac{\rho C L}{\alpha}$$

where

ρ = density of gage material

C = specific heat of gage material

L = gage thickness

α = temperature coefficient of resistivity

E_o = initial voltage across gage

Since the bulk properties of the gage material are well known, the coefficient K can be easily calculated and the gage response established without an extensive calibration procedure. The temperature coefficient of resistivity, α, has been checked experimentally, however, in previous studies.

Stagnation point radiant heat energy flux has been measured by means of a newly devised technique which involves the use of a cavity gage as shown in Figure 8. Depending on the proper design of the entrance and the location of the cavity gage within the hemispherical model, almost all of the radiant energy originating from a known volume of the highly heated gas cap and incident upon the cavity entrance slit is absorbed within the internal walls of the gage. In addition, the electrons generated by high energy photons will be prevented from escaping. The energy entering the cavity gage will be absorbed by the thin (about 0.2μ) platinum film deposited on its internal surfaces. By segmenting the gage as shown in Figure 8 the one-dimensionality of its operation is preserved and its sensitivity thereby increased considerably. Due to limited size of the model for this study (as dictated by the blockage effect in the 2" internal diameter shock tube) the test configuration allowed only the measurement of radiation along the stagnation streamline with a gage arrangement shown in Figure 9.

SHOCK TUBE PARAMETERS

Using the equilibrium thermodynamic properties computed by Browne (Ref. 5) for the established two gas mixtures, one with the nominal

content of 9% CO_2, 90% N_2 and 1% A and the other with 25% CO_2, 74% N_2 and 1% A, various gas dynamic properties associated with traveling and stationary shock fronts were calculated and charted as functions of shock velocity and the driven tube initial pressures.

The tabulated values of the equilibrium thermodynamic properties were plotted and the solution of the Rankine-Hugoniot shock relations obtained. All calculations were made for three initial driven tube pressures of P_1=1 mm, 5 mm and 25 mm of Hg. The initial driven tube temperature, T_1, was taken to be 294°K. The range of shock velocities, U_s, between 10,000 ft/sec and 30,000 ft/sec was covered. However, due to the limited range of the available thermodynamic properties which extended only up to 15,000°K some of the shock tube parameters could not be calculated for all velocities.

a. Incident Shock

The state of the gas on both sides of a normal shock is related by three basic equations corresponding to the physical principles of the conservation of mass. momentum and energy. These are:

$$u_2 = u_s \left(1 - \frac{\rho_1}{\rho_2}\right)$$

$$P_2 - P_1 = \rho_1 u_s^2 \left(1 - \frac{\rho_1}{\rho_2}\right)$$

$$h_2 - h_1 = \frac{1}{2} u_s^2 \left[1 - \left(\frac{\rho_1}{\rho_2}\right)^2\right]$$

where   h = enthalpy

         p = pressure

         u = velocity

         ρ = density

and subscripts 1 and 2 refer to regions ahead and behind the incident shock.
The simultaneous solution of these equations together with the available
tabulation of the equilibrium state produces results which are plotted in
Figures 10, 13, 16, 19, and 21   for the 9% CO_2 mixture and in
Figures 22, 25, 28, 31, and 33   for the 25% CO_2 mixture.

   b. Stationary Normal Shock (Laboratory Coordinates)

   After the passing of the incident shock the model finds itself in a
supersonic quasi-steady flow with the properties of region 2 ahead of the
model bow shock wave. The flow close to the axis of symmetry is decelerated
to subsonic velocity. The state of the gas along the stagnation streamline on
both sides of the bow shock is governed by the same three conservation laws.

$$\rho_2 u_2 = \rho_3 u_3$$

$$P_3 - P_2 = \rho_2 u_2^2 \left(1 - \frac{\rho_2}{\rho_3}\right)$$

$$h_3 - h_2 = \frac{1}{2} u_s^2 \left[1 - \left(\frac{\rho_2}{\rho_3}\right)^2\right]$$

where subscript 3 refers to the region behind the bow shock. The calcula-
tion produced the results which are presented in Figures 11, 14, 17,
20   for the 9% CO_2 mixture and in Figures 23, 26, 29, and 32 for
the 25% CO_2 mixture.

c. Stagnation Region

The flow along the stagnation streamline in region 3 is decelerated to a stop at the body. The stagnation conditions are found as follows: The enthalpy is given directly by $h_s = h_3 + 1/2 \, U_3^2$. The stagnation pressure is computed approximately by assuming incompressible flow $P_s = P_3 + 1/2 \, \rho_3 \, U_3^2$. Both the stagnation temperature and the corresponding density are read off directly from the thermodynamic state charts and plotted in Figures 12, 15, and 18 for 9% CO_2 mixture and in Figures 24, 27 and 30 for the 25% CO_2 gas.

d. Composition of Stagnation Region Gas

The equilibrium concentration of the various species appearing in the dissociated and ionized gas when heated to the enthalpy level corresponding to the stagnation point had also been obtained and plotted as a function of shock velocity. These are shown in Figures 34 through 37 for both the 9% and 25% CO_2 mixtures and for the two test cases of $P_1 = 1$ and 5 mm Hg. Electron concentration for pure CO_2 and pure N_2 are also included in Figures 38 and 39 respectively.

e. Radiant Heat Flux to the Stagnation Point

The radiation heat flux to the stagnation point of the 1/2 in. diameter model was calculated using appropriate emissivities obtained for the heated atmospheres of Venus (Ref. 6). The stagnation point region was replaced by an infinite slab at a uniform temperature, T_s, and density, ρ_s, whose thickness, δ, is the shock stand off distance given by

- 11 -

$$\frac{\delta}{R_N} = \frac{2/3}{\frac{\rho_3}{\rho_2} - 1}$$

where R_N = radius of the hemispherical model.

The calculations were done for both atmospheric models and for three driven tube initial pressures. The results are presented in Figures 40 and 41.

RESULTS AND DISCUSSION

In the simulation of hypersonic flight situations at the stagnation point of a model in the shock tube the corresponding stagnation enthalpy and pressure are produced in a different manner than in the flight case. The test gas is first compressed and accelerated by the incident shock wave generated when the diaphragm dividing the driver and the driven tube is ruptured. The flow behind the shock front, although moving with high velocity, is only slightly supersonic due to the high temperature or high sonic velocity in the gas processed by the advancing incident shock wave. This gas will now flow around our model. Since a blunt body is being investigated, a detached bow wave will be established. The gas along the stagnation streamline will undergo compression essentially across a normal shock and finally will be stagnated at the surface of the body.

As long as the boundary layer thickness is small in comparison with the shock layer whose measure at the stagnation point is the detachment distance, the boundary layer problem can be considered separately from the inviscid flow field and hence independently of the Reynolds number. The

only requirements for accurate simulation are the stagnation enthalpy, the velocity gradient at the stagnation point, and gas equilibrium in the various flow processes. For the hemispherical body the Newtonian approximation predicts that the velocity gradient is independent of Mach number. This has been confirmed experimentally. The correlation for the heat transfer rate through the laminar boundary layer at the stagnation point can be written

$$\dot{q}\sqrt{\frac{R_N}{P_s}} = f(h_s - h_w)$$

where R_N is body nose radius

h_w is wall enthalpy

Thus, the environment created in a shock tube can be directly applied to the solution of the stagnation point heating problem.

The performance of the shock tube in the mixtures of CO_2, N_2 and A does not differ appreciably from its performance in air. Maximum shock velocities obtained during this experimental program for P_1 values of 5 mm and 1 mm Hg were approximately 24,500 ft/sec and 30,200 ft/sec. In both cases maximum capacitor energy (about 50,000 joules) was discharged in the driver for heating the helium.

The constituent concentrations of the mixtures tested differed slightly from the nominal values listed earlier.

Comp. Model	Nominal	Actual
I	9% CO_2, 90% N_2, 1% A	8.80% CO_2, 89.98% N_2, 1.22% A
III	25% CO_2, 74% N_2, 1% A	25.10% CO_2, 73.78% N_2, 1.12% A

The test gas mixtures were considered to be sufficiently close to the specified values to satisfy the objectives of the study.

During each run, wall pressure histories behind the incident shock wave were recorded. A typical oscillogram of signal from a pressure gage located at position five is shown in Figure 42, corresponding to a shock velocity U_s = 20,300 ft/sec and initial tube pressure of 5 mm Hg. The effect of boundary layer growth behind the incident wave is indicated by the side wall pressure rise with time. Note that this rise is small during the passage of the test gas, however. Pressure traces of the type shown in Figure 42 are complicated by large oscillations caused by the response of the gage and associated electronic circuits. They are used primarily to verify the test pressure level and to qualitatively interpret the phenomena occurring in the tube process (arrival of expansion wave - not seen in Figure 42 - and boundary layer effect on pressure level, for example).

The heat transfer measurements were made at the stagnation point of a 0.5 in. diameter hemisphere-cylinder model using a calorimeter heat transfer gage (Ref. 7). The gage material used for the 0.5 in. diameter model was .004 in. thick Hytemco. A few experiments were performed with a 0.75 in. diameter model and the gage used 0.003 in. thick platinum. According to the analytical results of Ref. 7, these thicknesses can only introduce a small error in the measured heating results. Their use is, therefore, justified by practical considerations. The oscillogram of the signals from both type gages are shown in Figures 44.a. and 44.b. respectively. The

The conditions of both tests were very similar. The shock velocities were 29,200 and 29,600 ft/sec, and the initial pressures 1 mm Hg in both cases. The first test was in 25% CO_2 mixture; the second, in air. Although in this particular case the noise level of the response of either gages seems to be of the same magnitude, closer examination of the traces will prove that the platinum gage response is cleaner. This was also observed in other runs. The initial jump of the DC level with the Hytemco gage was also observed to occur with the platinum gage. Lack of similarity of the precursor response during the two or three microseconds before shock arrival cannot be explained at present.

The oscillogram from a calorimeter heat gage at the stagnation point of the 0.5 in. model is shown in Figure 43. The instantaneous rate of change of the output together with the known properties of the Hytemco alloy gives the unknown heat rate for a given time interval. A corresponding trace of the optical pyrometer sensing the radiation across the incident shock of station five is also shown. Taking the time interval during which the intensity of radiation is level and allowing for the formation of the bow shock (2 to 3 μs), the useful test time was arrived at and the slope of the gage signal during that period was measured, giving the unknown heat transfer rate.

The experimental study involved a series of runs in the 9% and 25% CO_2 mixtures over a wide shock velocity range (note that U_s does not equal U_f), simulating hypersonic entry at altitudes between 240,000 and 260,000

ft. of the atmospheric model I. The results are shown in Figure 45.

Points marked by circles and triangles are from tests in 9% and 25% CO_2 mixtures, respectively. In addition, some data obtained in pure CO_2 and N_2 are included. The limited results in CO_2 heat transfer measurements of Rutowski and Chan (Ref. 8) at low enthalpies are also entered.

The theoretical curves representing Scala's calculation of equilibrium boundary layer for dissociated and ionized nitrogen are drawn together with his early estimated region of uncertainty for partially ionized carbon dioxide. At $(h_s - h_w)$ values below 24, 000 BTU/lb the experimental data follow the theoretical curve. At higher enthalpies the present data give heat transfer rates somewhat lower than the ionized theory for N_2. The pyrometer records indicate that the simulation of flight velocities below 35, 000 ft/sec gives valid data with sufficient test time. The results corresponding to higher flight velocities may have insufficient test time for accurate readings. This limitation is more likely to exist for the CO_2 mixtures than for air and nitrogen because of the apparent long relaxation times for the non-equilibrium process behind the incident shock wave (see Figure 43). Such an effect could cause the observation of values lower than actually exist and is, therefore, quite important. This possible restriction on the results is imposed by the present 2" test facility and will be remedied by the installation of the 6" shock tube scheduled for operation shortly.

It is interesting here to note that the electron densities of the stagnation point as calculated for 9% and 25% CO_2 mixtures, pure N_2 and pure CO_2

differ little from each other; this can be seen in Figures 34 through 37.

The contribution of radiation to the measured heat transfer rate was calculated and, in the case of both gas mixtures, its magnitude is less than 8% assuming complete absorption by the gage surface. This is the theoretical upper limit of possible radiative error in the measured boundary layer heating. Figure 46 shows the response of the cavity radiation gage during a test run in the 25% CO_2 mixture. It is pointed out that the sensing element in the cavity gage is a thin film surface temperature resistance thermometer so that its response is different from that of a calorimeter gage. For example, for a constant heating pulse applied in a step function at $t = 0$, the thin film response will be proportional to $\sqrt{t}$ while the calorimeter response will be proportional to t. The signal shown exhibits some electronic noise just prior to shock arrival over a time period similar to that observed with the calorimeter gage traces. Again, this is undoubtedly due to rapid charge equilibration about the model in the ionized flow. The physical mechanisms causing these early signals are not clear; however, it again appears that they become unimportant soon after the shock wave reaches the model. The relatively clean response of the gage during approximately the 10 μ sec following the shock wave arrival indicates that this is the time for passage of the shocked test gas. The subsequent fall and rise are responses to the irregular driver gas flow that then impinges on the model. Note that a drop in response is an indication of suddenly reduced heating rate. The radiative heating rate at the stagnation point corresponding to

the gage signal shown in Figure 46 has not yet been reduced accurately. However, an approximate reduction shows it to be within 30% of the calculated value. Therefore, the conclusion is drawn that the radiation contribution to measured heating rate values is small (10% or less). This conclusion is now based upon both experimental and theoretical grounds.

CONCLUSIONS

The experimental program of stagnation point heat transfer rate measurement on a blunt body in two simulated atmospheres of Venus supplied data which indicate that within the experimental accuracy no discernible difference between the heat transfer rate in 9% CO_2 mixture and in the 25% CO_2 mixture can be observed. For conditions corresponding to flight velocities below 35,000 ft/sec the experimental data agree well with theory. For higher values of (h_s - h_w) or corresponding flight velocities the test results may suffer due to short test time caused by slow approach to equilibrium of reaction processes behind the normal shock. The new 6" shock tube now in process of installation will increase considerably the available test time. Calculation of the upper limit of equilibrium radiation from the shock layer to the stagnation point indicates that its contribution to the measured rates is small. Measurement of the radiation by the newly developed total radiation gage gives values close to the theoretical prediction.

Further studies of equilibrium and non-equilibrium radiation and the influence of non-equilibrium flows on the convective heat transfer rate are recommended. The behavior of the laminar and turbulent boundary layers and the transition phenomena should also be studied in the hypervelocity shock tube facility.

ACKNOWLEDGEMENTS

REFERENCES

1.   Resler, E. L., Lin, S. C., and Kantrowitz, A.; The Production of High-Temperature Gases in Shock Tubes; JAP 23, No. 12 (1952).

2.   Rose, P. H., and Stark, W. I.; Stagnation Point Heat Transfer Measurements in Dissociated Air; JAS 25, No. 2 (1958) February.

3.   Hollyer, R. N., Hunting, A. C., Laporte, O., and Turner, E. B.; Luminosity Generated by Shock Waves; Nature 171, 395 (1953).

4.   Warren, W. R., Rogers, D. A., and Harris, C. J.; The Development of an Electrically Heated Shock Driven Test Facility; Second Symposium on Hypervelocity Techniques, University of Denver, Denver, Colorado, March, 1962.

5.   Browne, W. G.; Thermodynamic Properties of the Venusian Atmosphere; Advanced Aerospace Physics Tech. Memo No. 13, (Three Parts), June 11, 1962.

6.   GE-MSD; Venus-Mars Capsule Study, JPL Contract 950250, (Two Volumes); July 30, 1962.

7.   Rose, P. H.; Development of the Colonimeter Heat Transfer Gage for Use in Shock Tubes; AVCO Research Report 17, February, 1958.

8.   Rutowski, R. W., and Chan, K. K.; Shock Tube Experiments Simulating Entry Into Planetary Atmospheres; LSMD-288139, January, 1960.
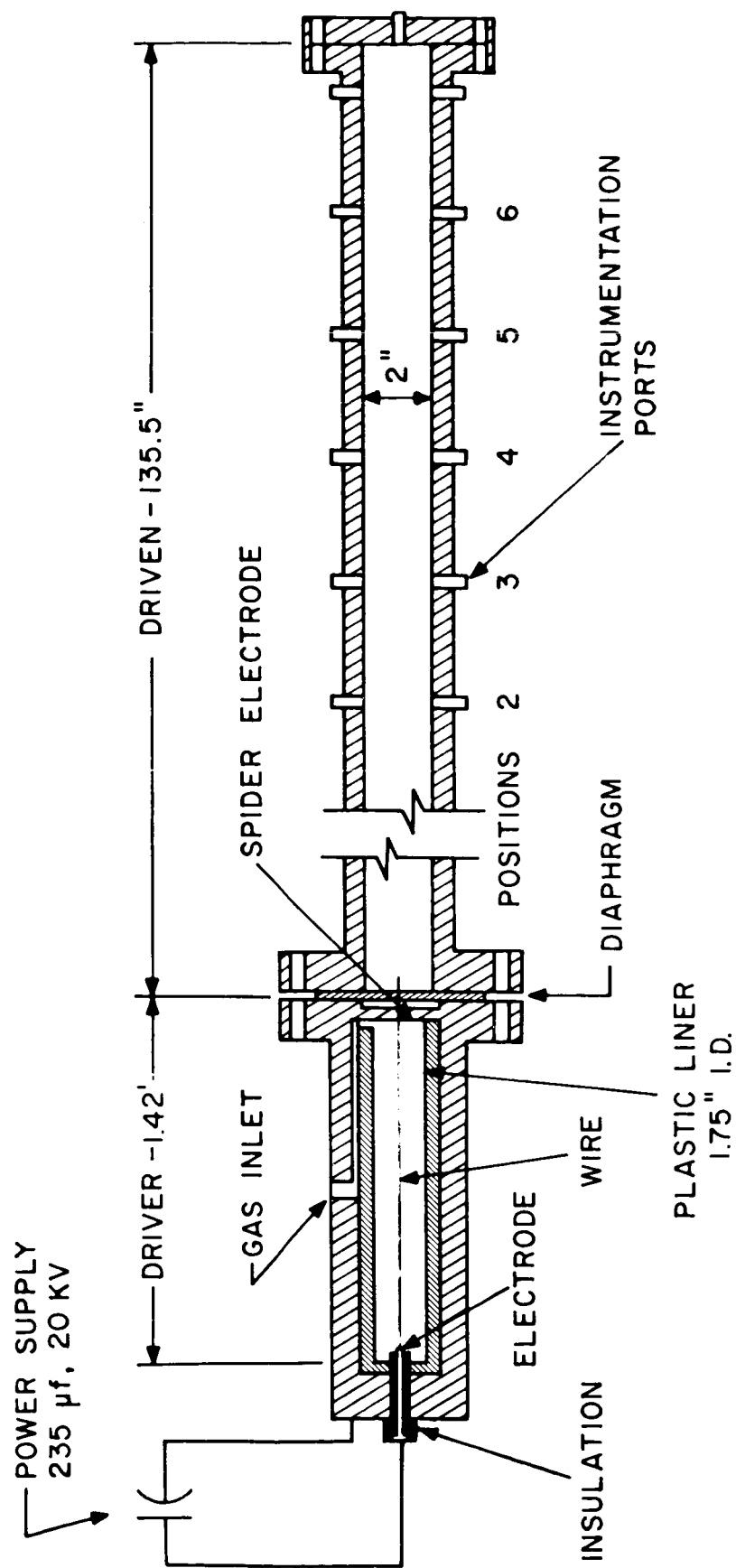
Figure 1. Design of Arc Heated Shock Tube
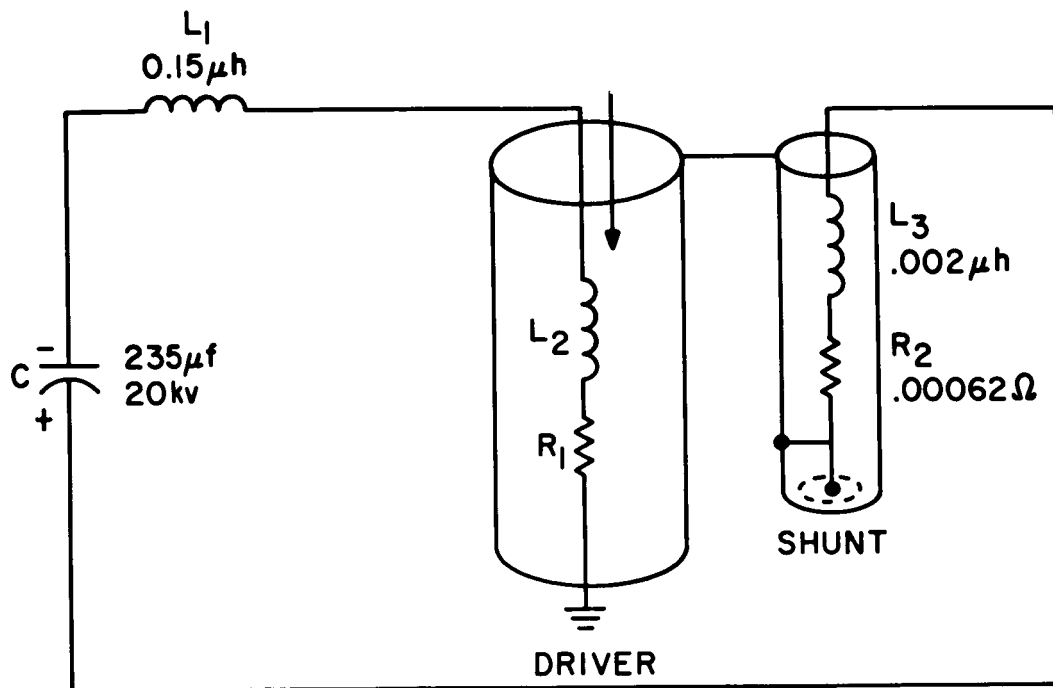
(a) CIRCUIT DIAGRAM
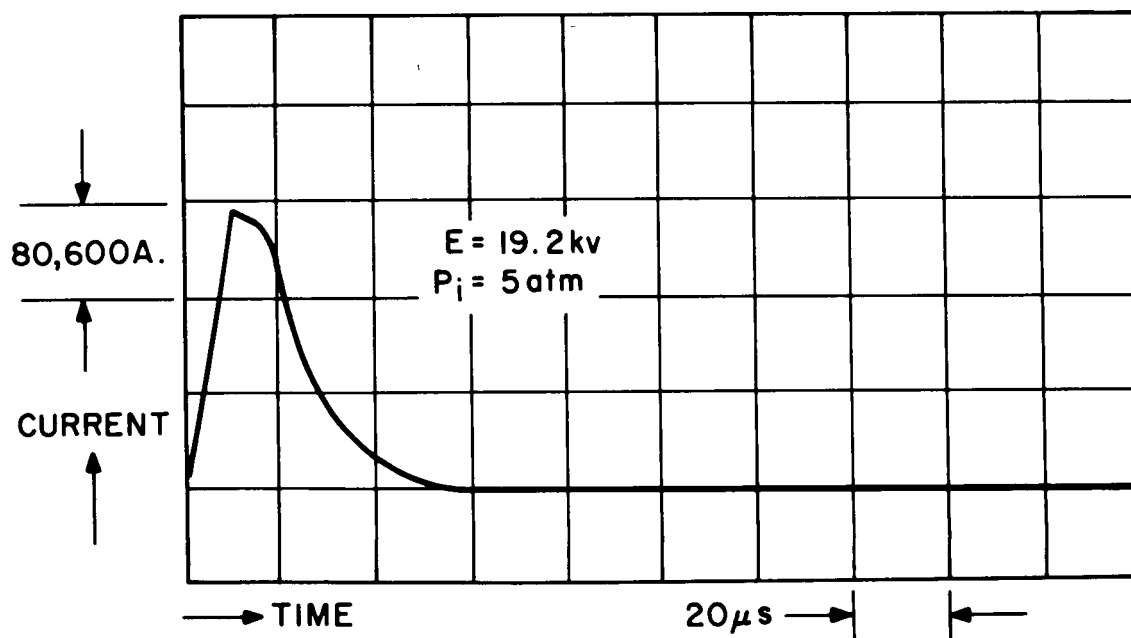
(b) CURRENT WAVEFORM

Figure 2. Typical Electrical Characteristics of Prototype Shock Tube
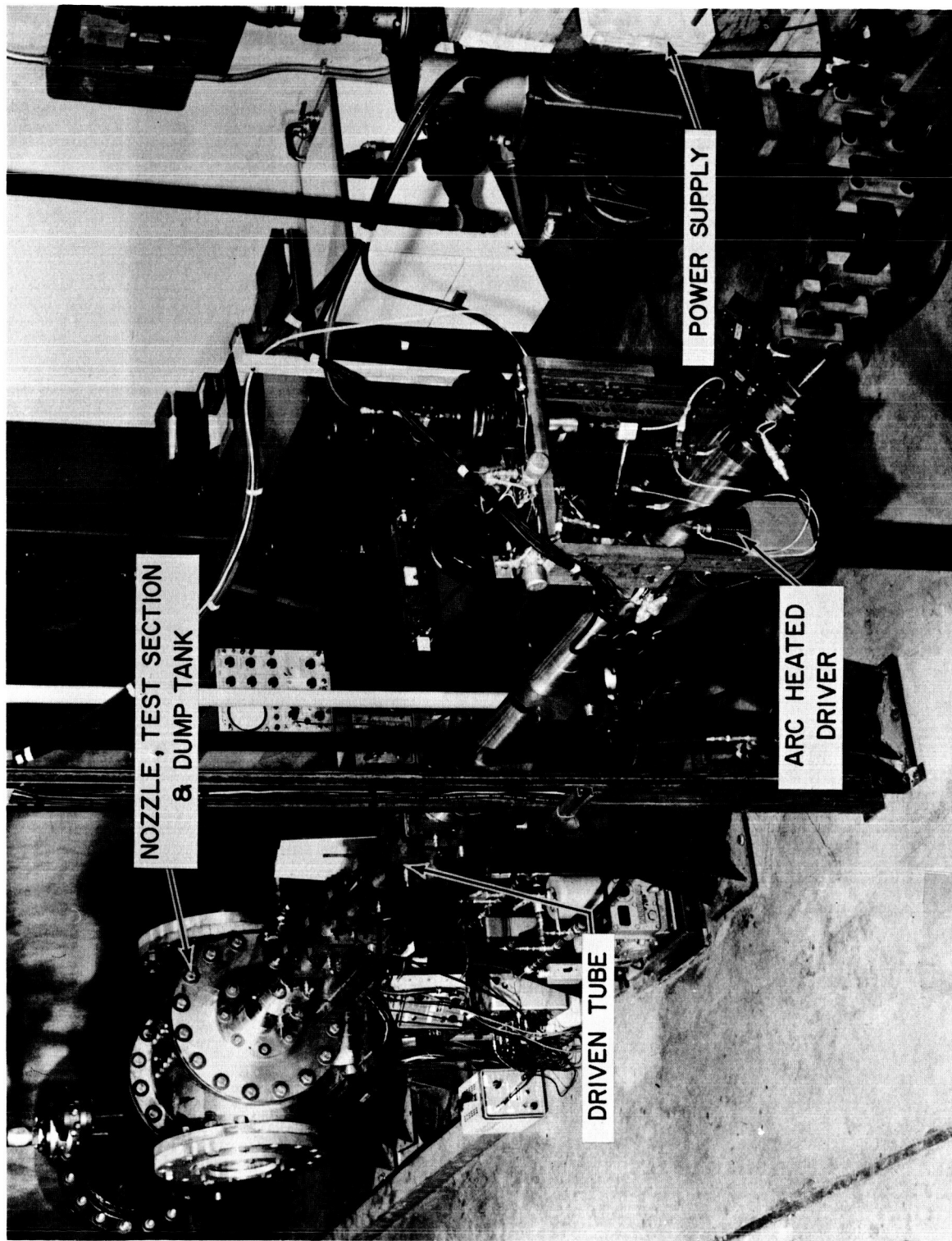
Figure 3. High Enthalpy Shock Tube Facility
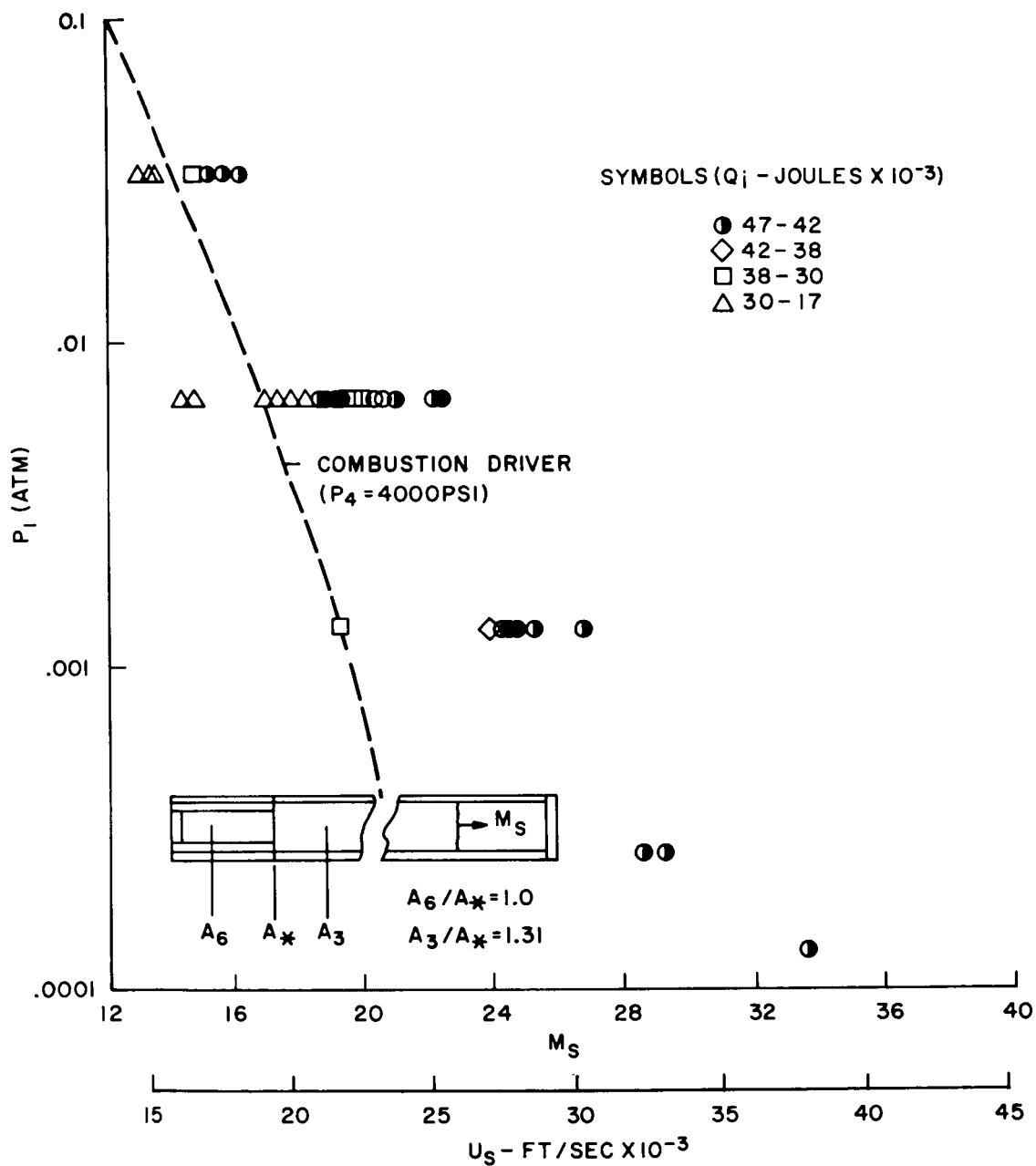
Figure 4.   Arc Heated Helium Driver Shock Tube, M_S vs. P_1

(2" Shock Tube - Max. Available Energy: 47,000 Joules)
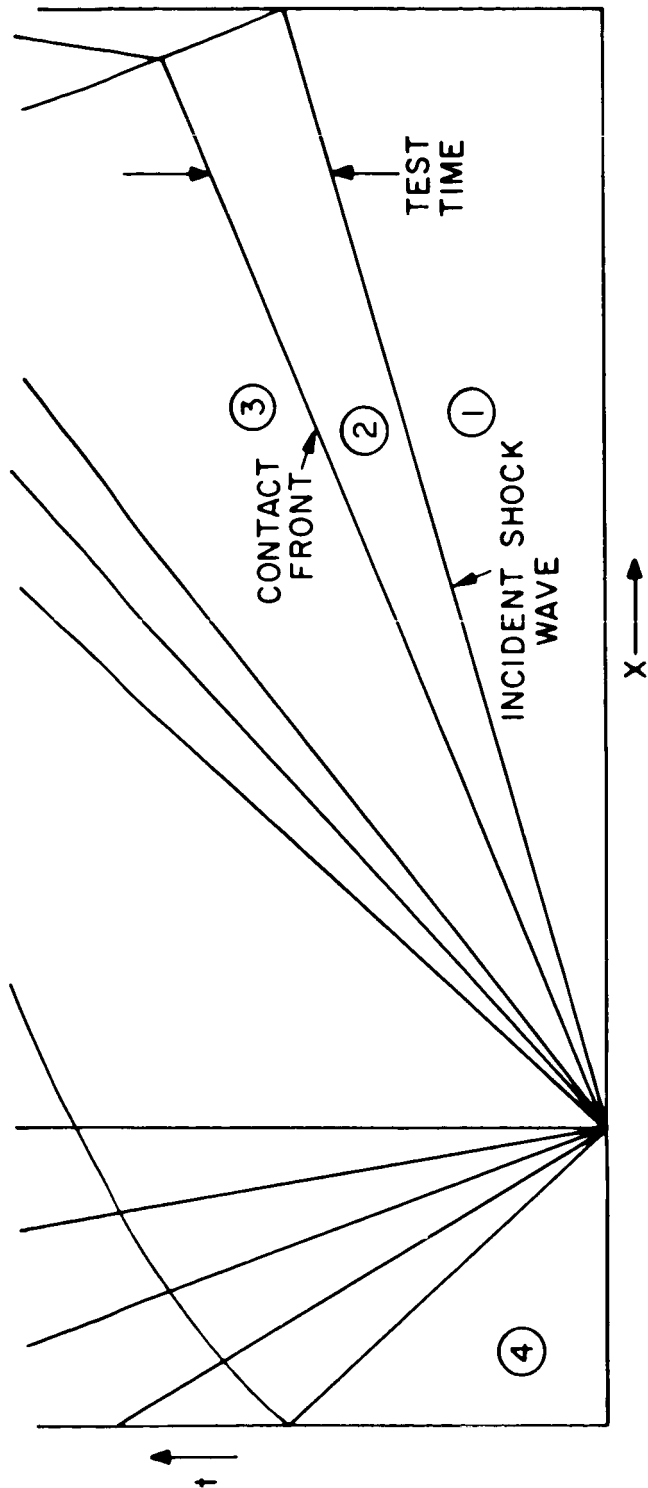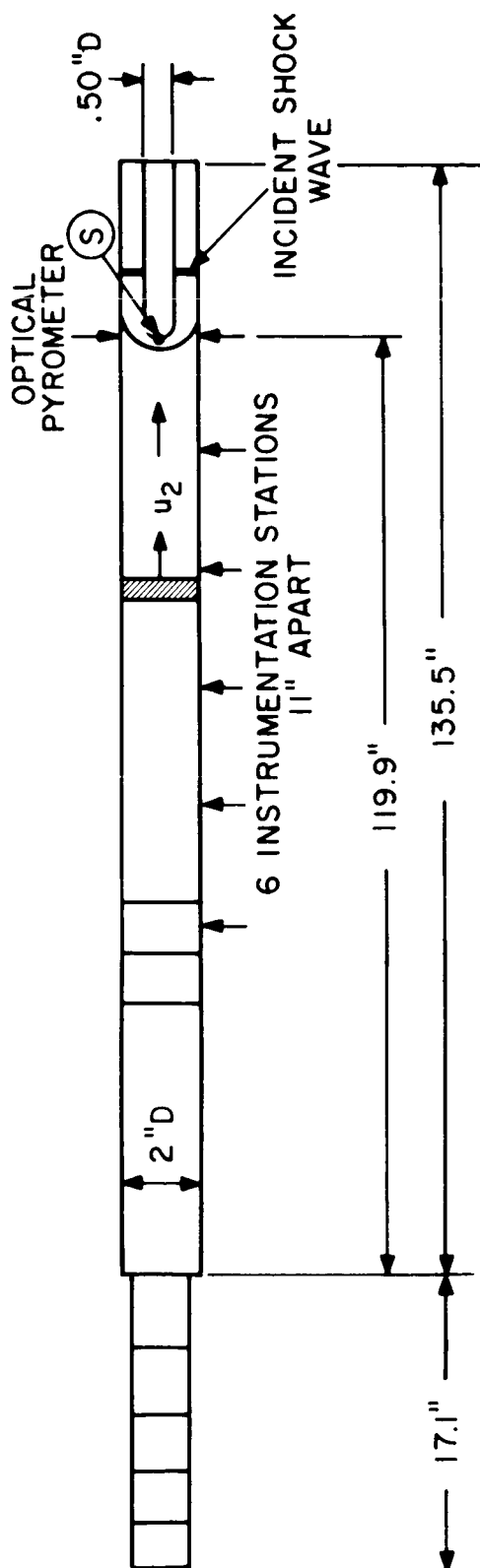
Figure 5. Straight Tube Test Configuration Model. Heat Transfer Measurements
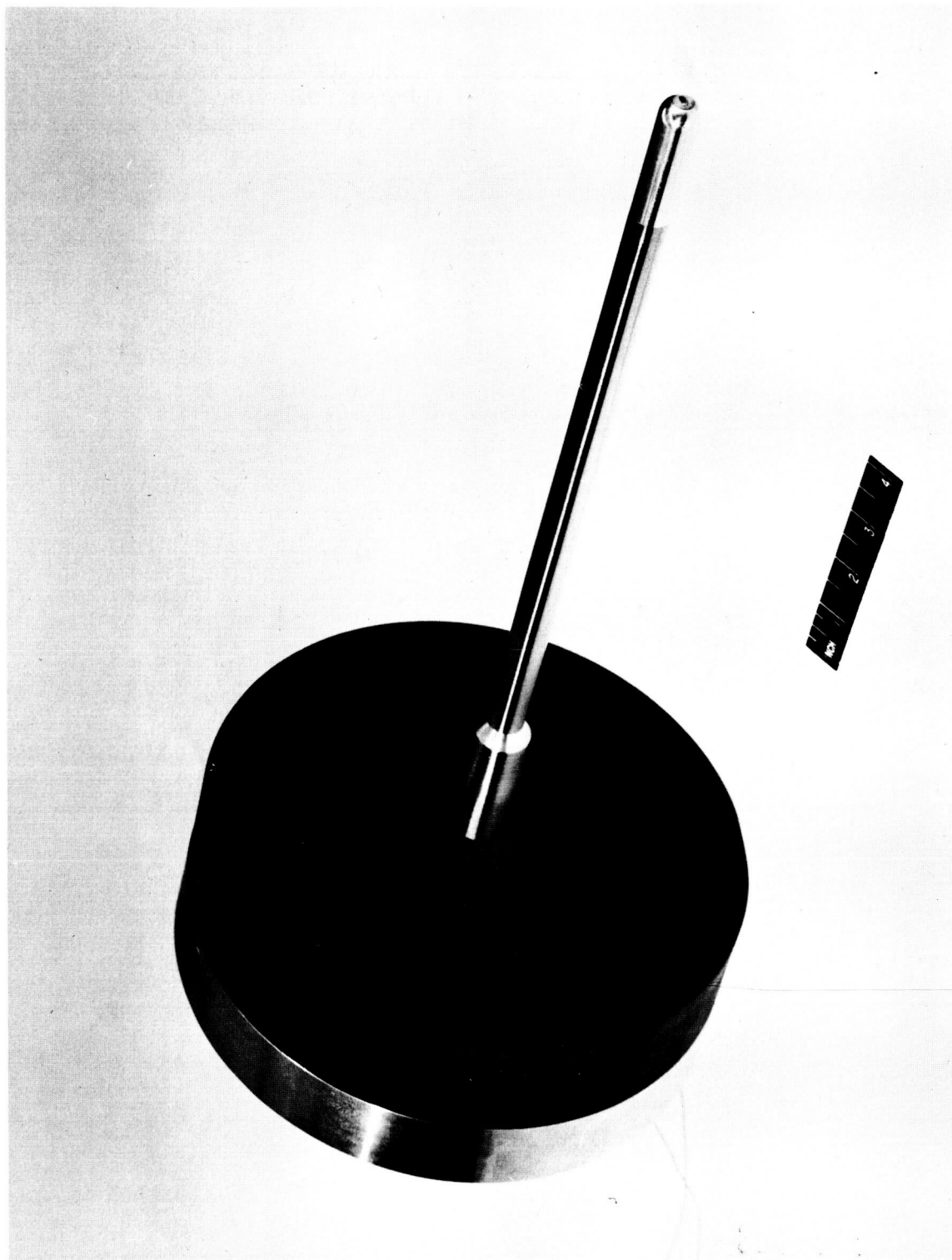
Figure 6. Half-inch Model with Heat Transfer Gage

a. CALORIMETER GAUGE

b. SCHEMATIC OF GAUGE CIRCUIT

Figure 7.   Heat Transfer Rate Measurement Set-up.

ADVANTAGES:
1. WINDOWLESS AND NO SURFACE EFFECT UNCERTAINTY. ACCEPTS AND MEASURES ALL INCIDENT RADIATION

2. COLLIMATION ALLOWS MEASUREMENT OF TOTAL EMISSION FROM LOCAL AREAS OF HEATED GAS WITH μs RESOLUTION.

THIN FILM ON INNER SURFACE

i_g

I

SCHEM. GAGE CIRCUIT

MOVING SHOCK WAVE

$u_2 \longrightarrow$ $\longrightarrow u_s$

$u_2 \longrightarrow$

MODEL STAGNATION REGION

Figure 8.   Cavity Gage for Total Radiative Heat Transfer Measurements

STING MODEL SUPPORT

CAVITY GAGE

WINDOW
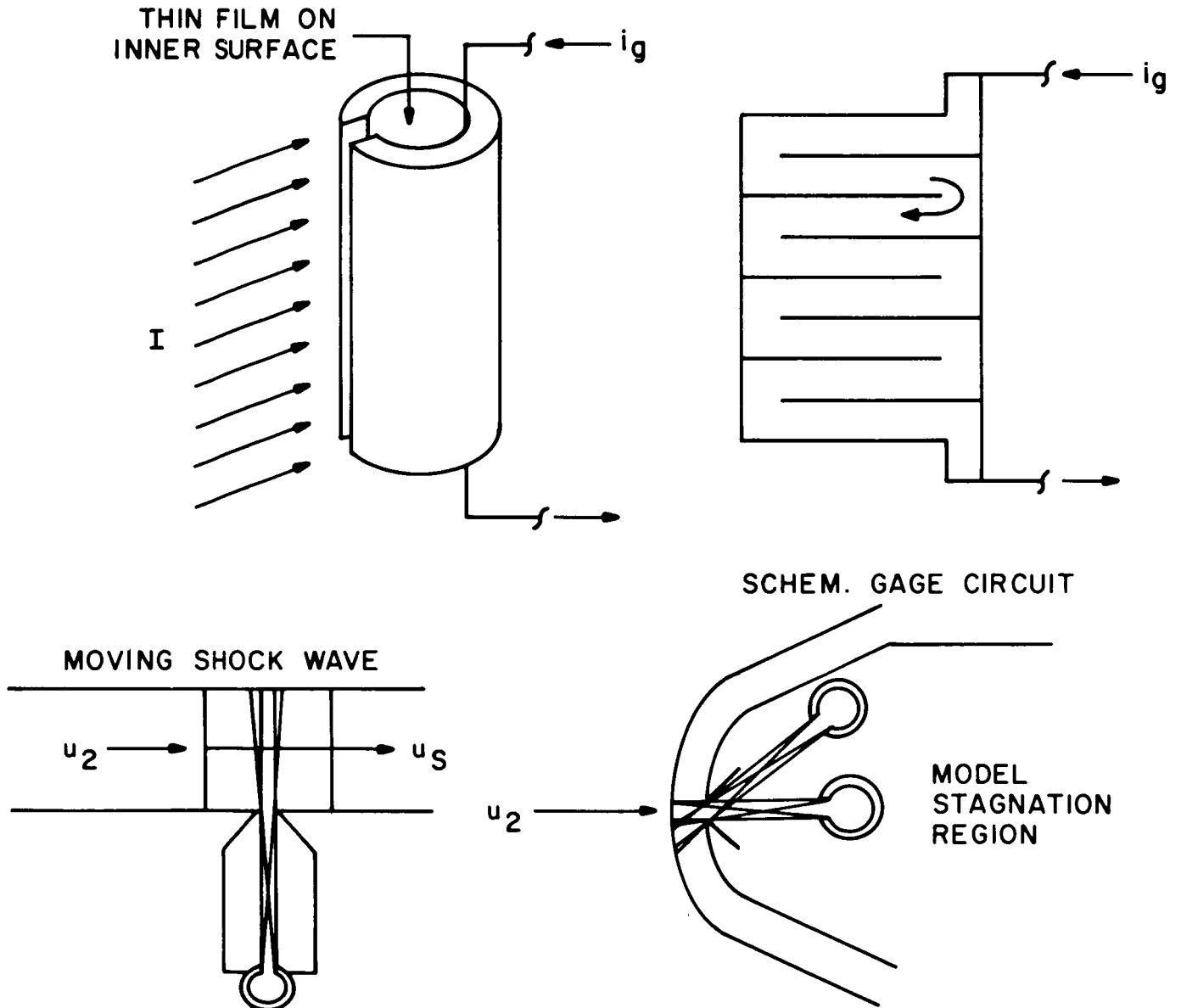
Figure 9. Total Radiation Gage
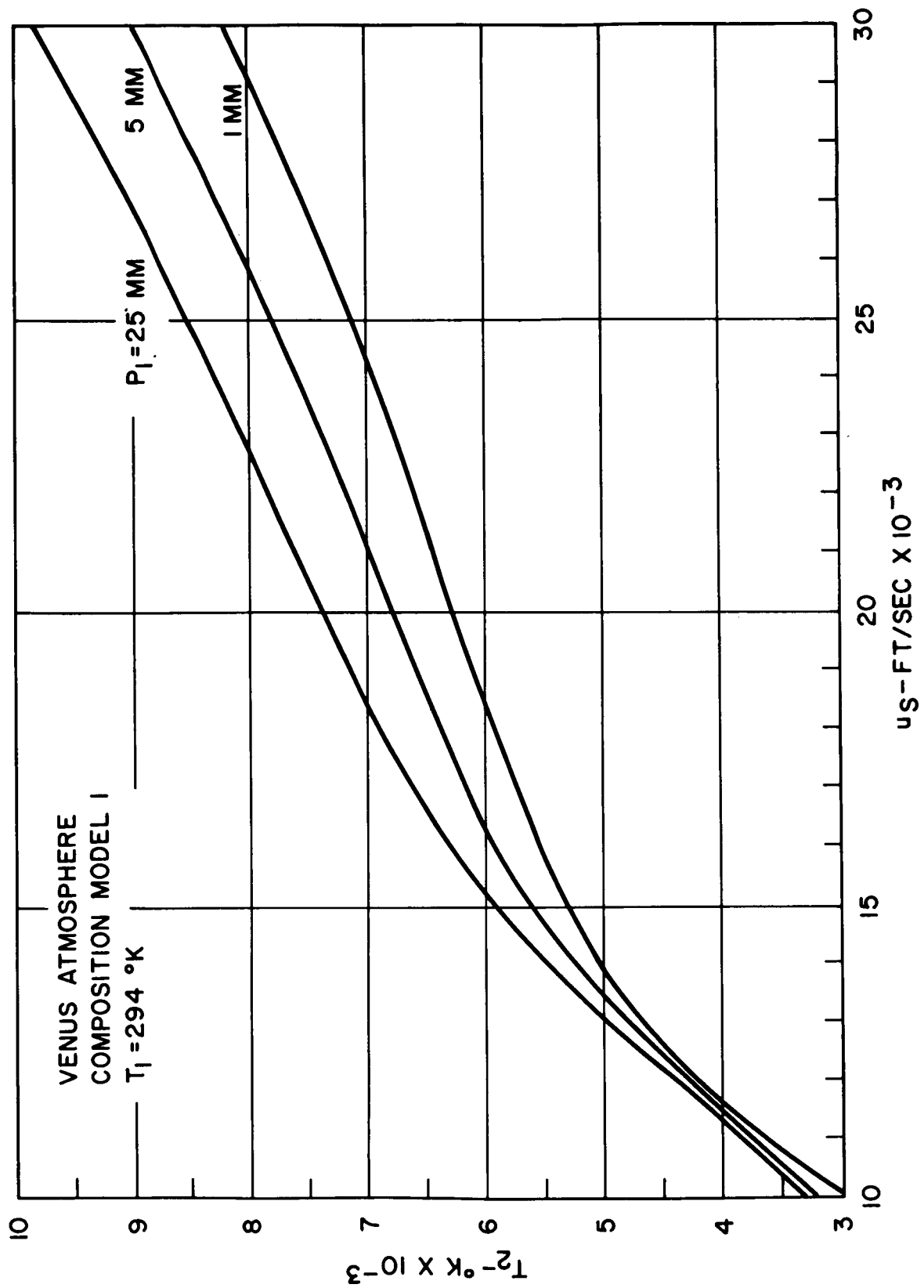
Figure 10.   Temperature Behind Incident Shock
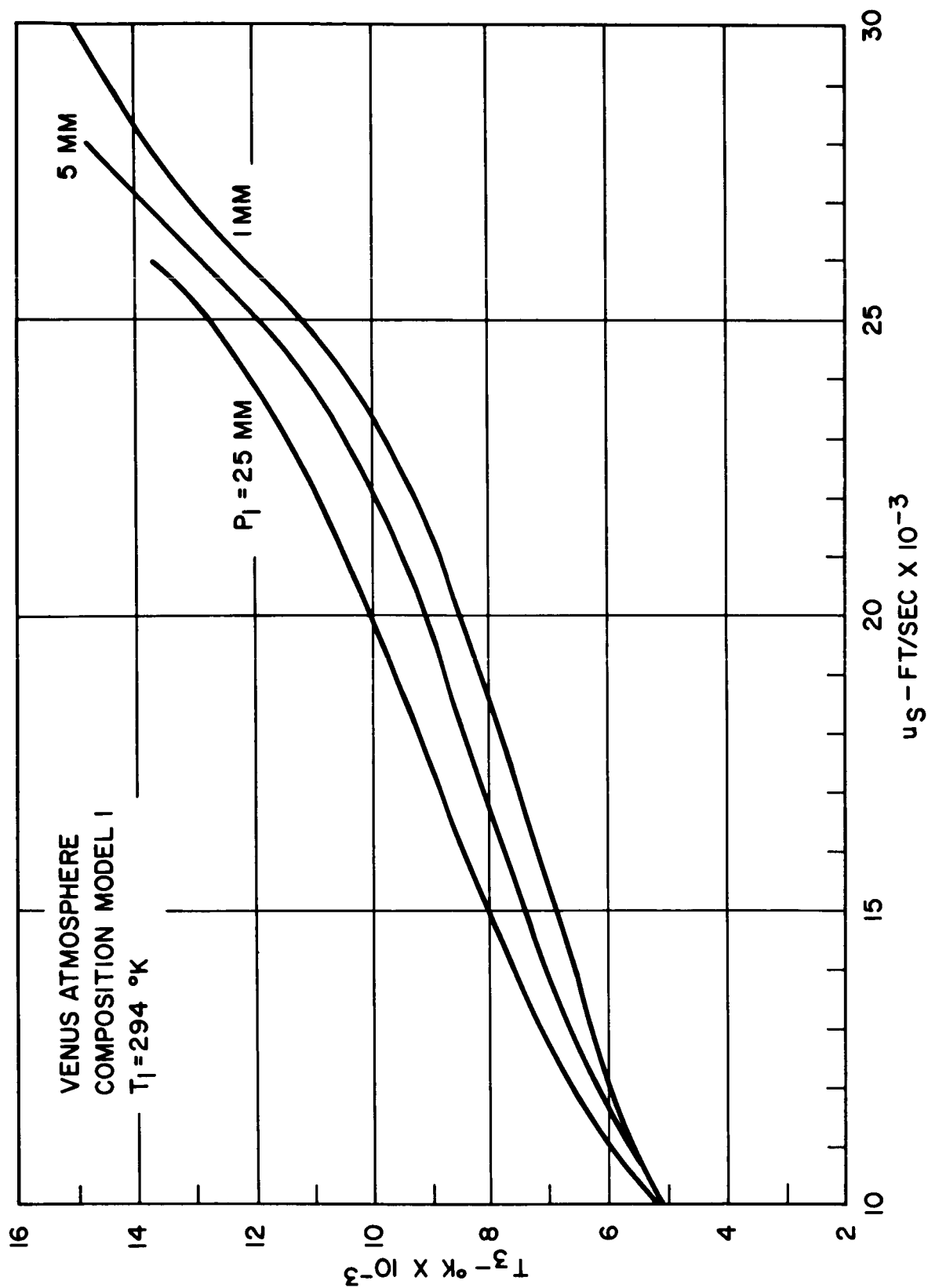
Figure 11. Temperature Behind Normal Shock
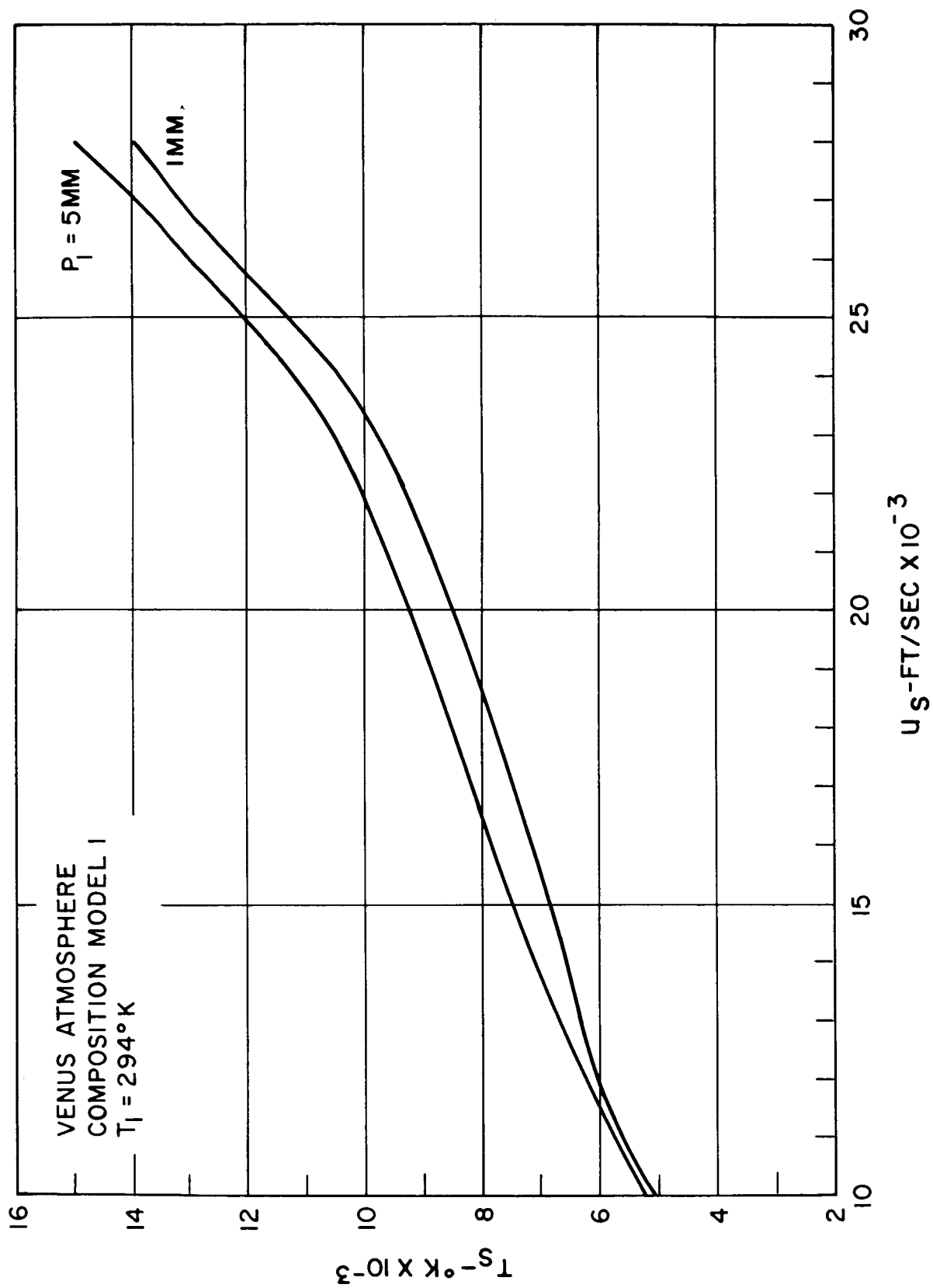
Figure 12. Stagnation Temperature
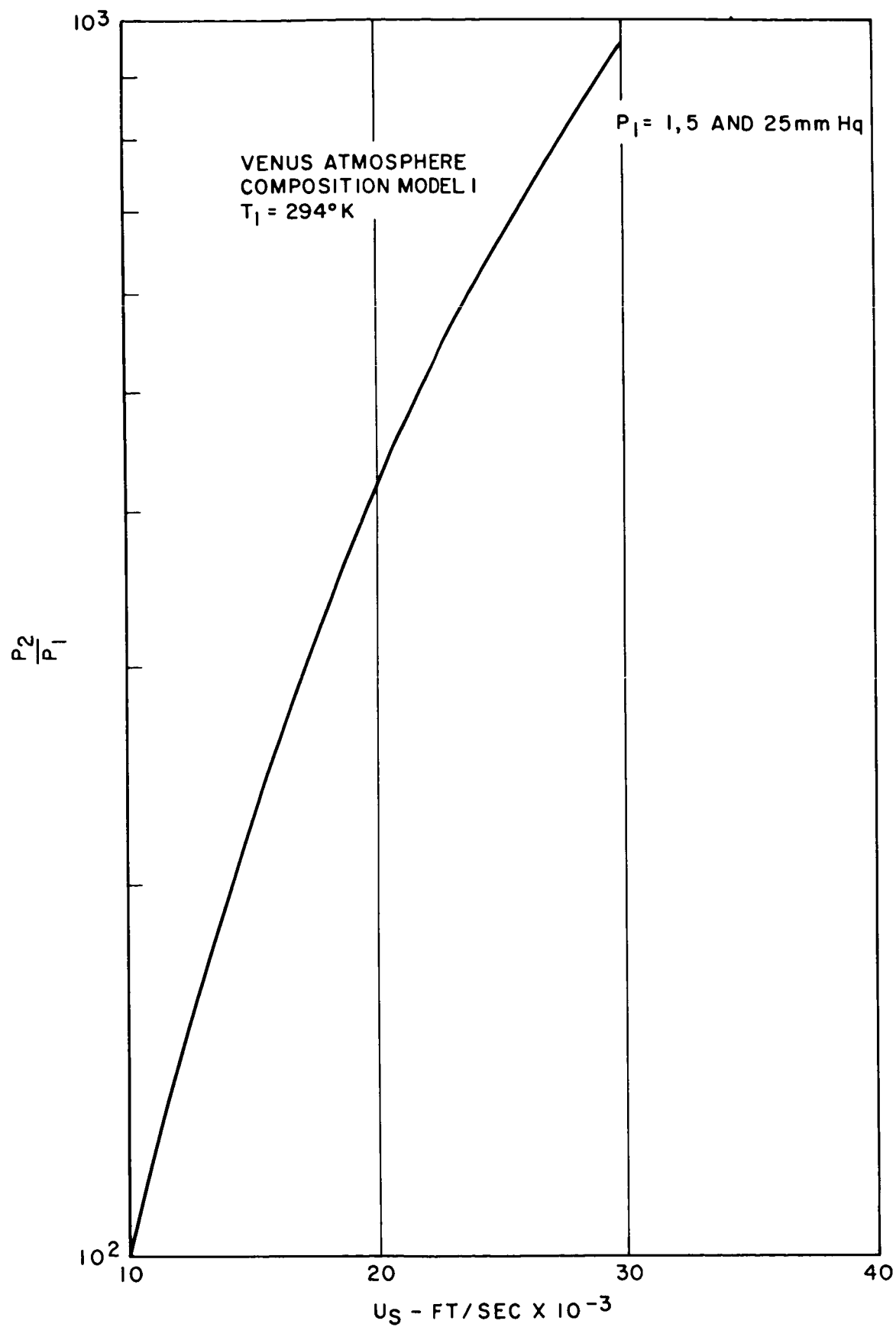
Figure 13. Pressure Behind Incident Shock
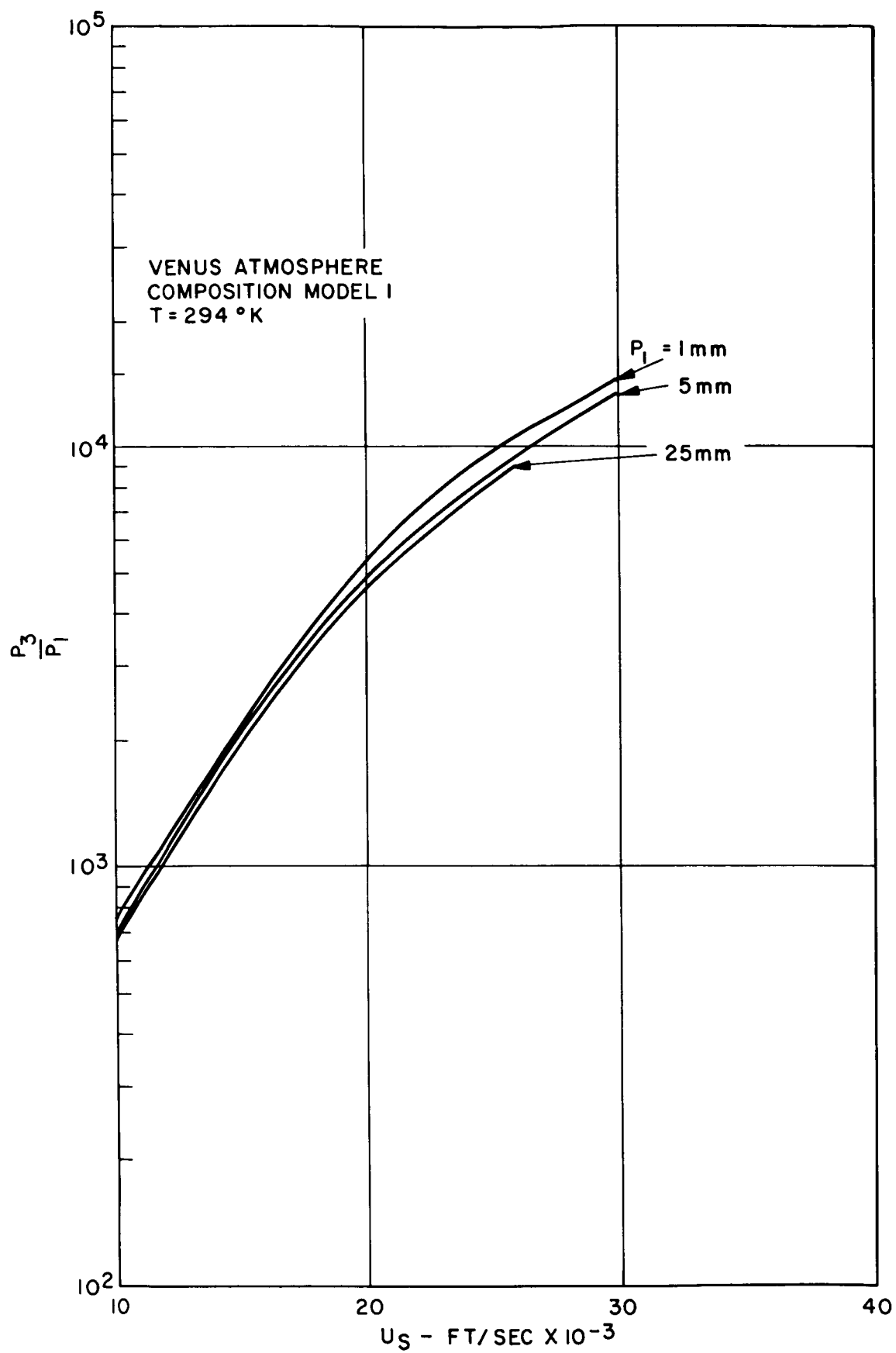
Figure 14.   Pressure Behind Normal Shock
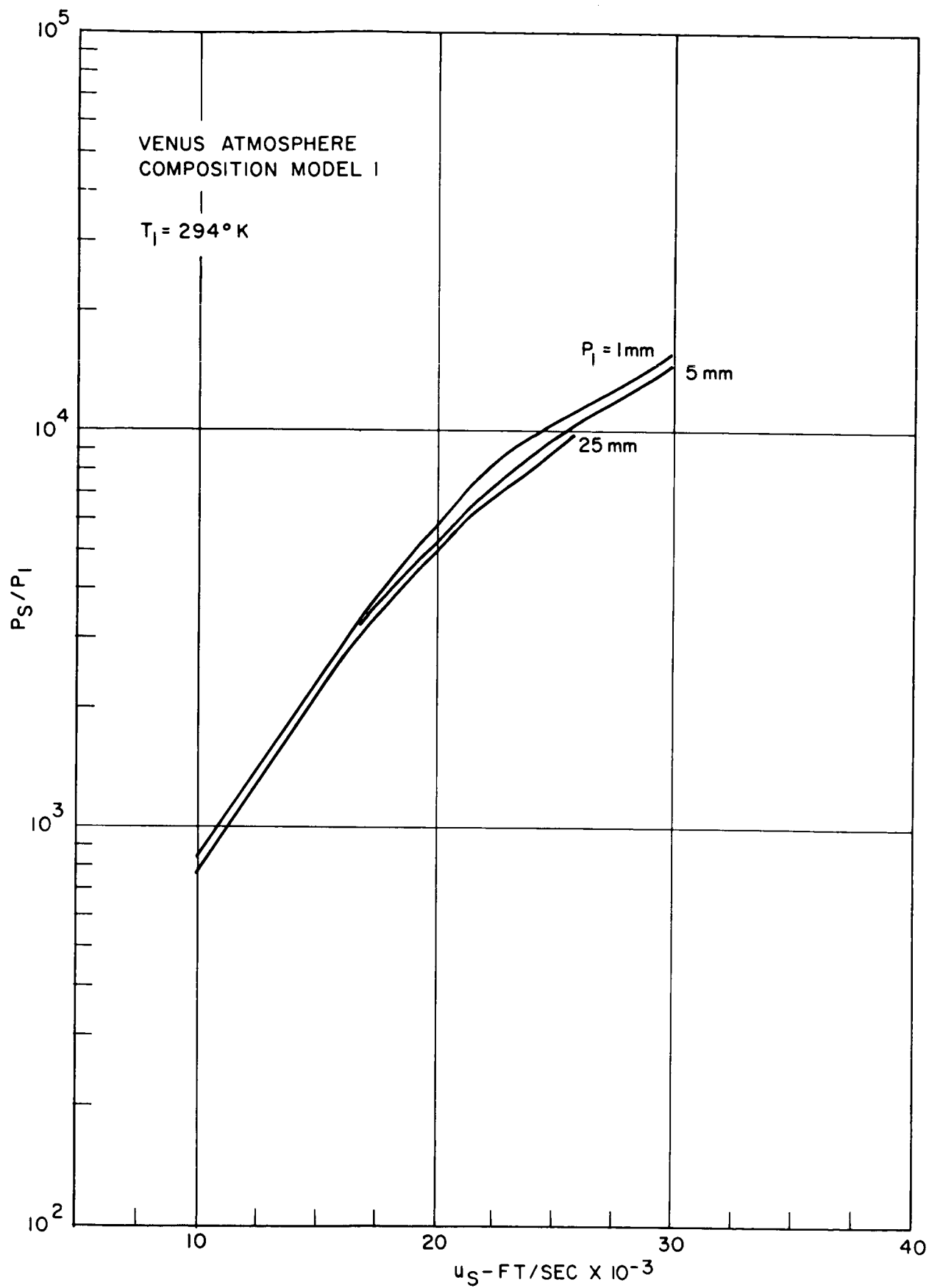
Figure 15. Stagnation Pressure
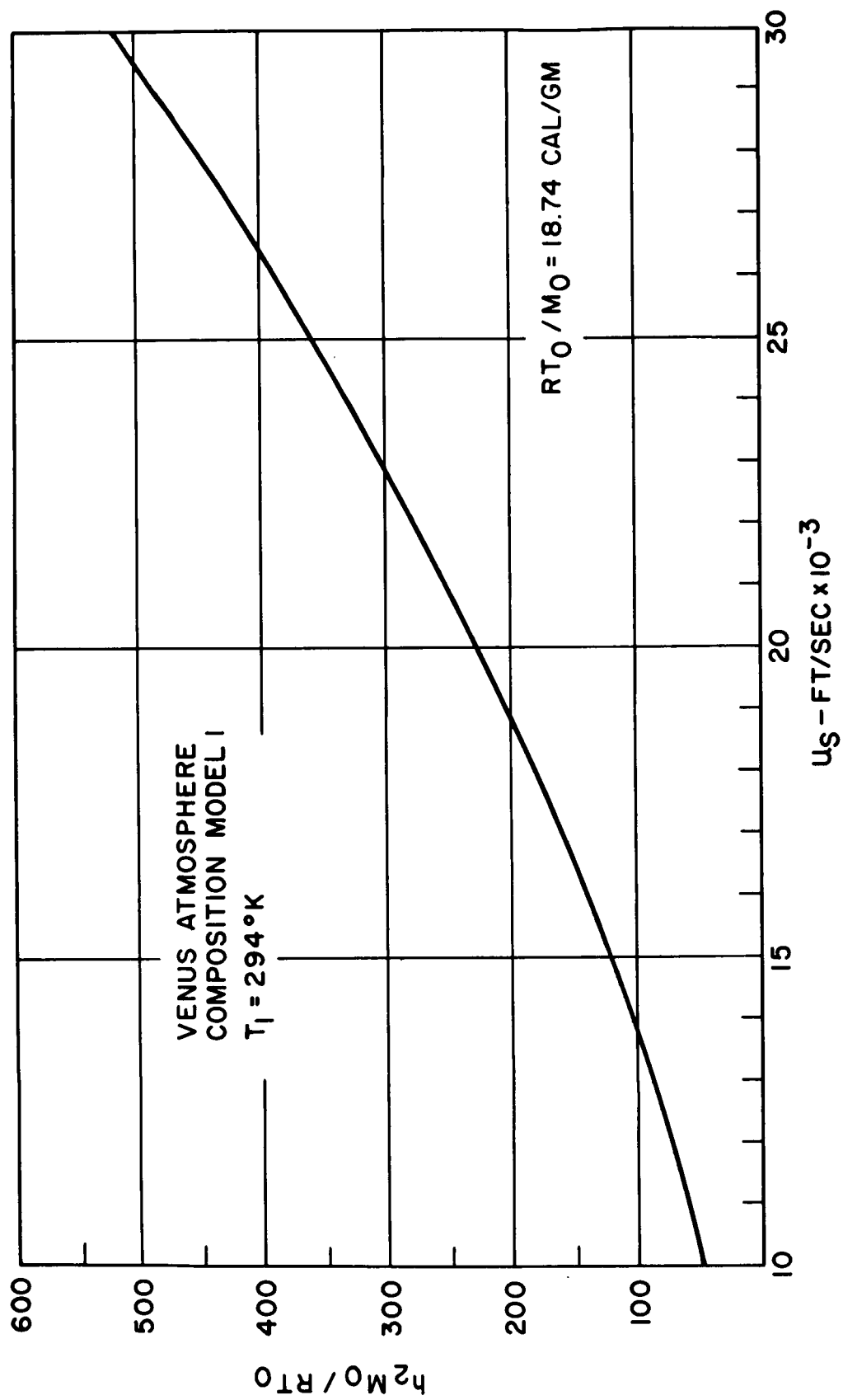
Figure 16.   Enthalpy Behind Incident Shock
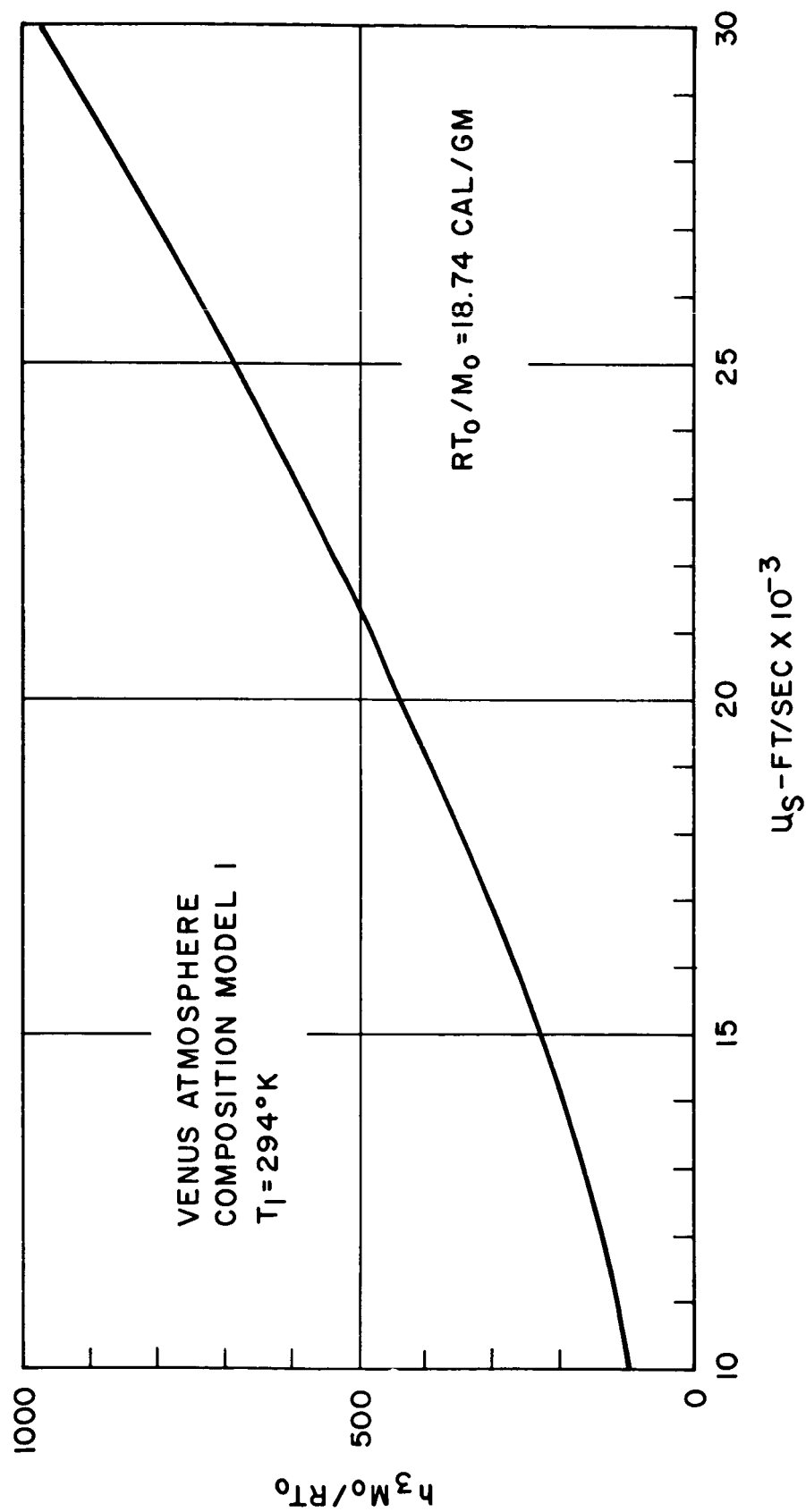
Figure. 17. Enthalpy Behind Normal Shock

Plot axes and labels:

Vertical axis (enthalpy): $h_3 M_0 / R T_0$, with values 0, 500, 1000

Horizontal axis: $u_S - FT/SEC \times 10^{-3}$, with values 10, 15, 20, 25, 30

VENUS ATMOSPHERE
COMPOSITION MODEL I
$T_I = 294°K$

$R T_0 / M_0 = 18.74$ CAL/GM
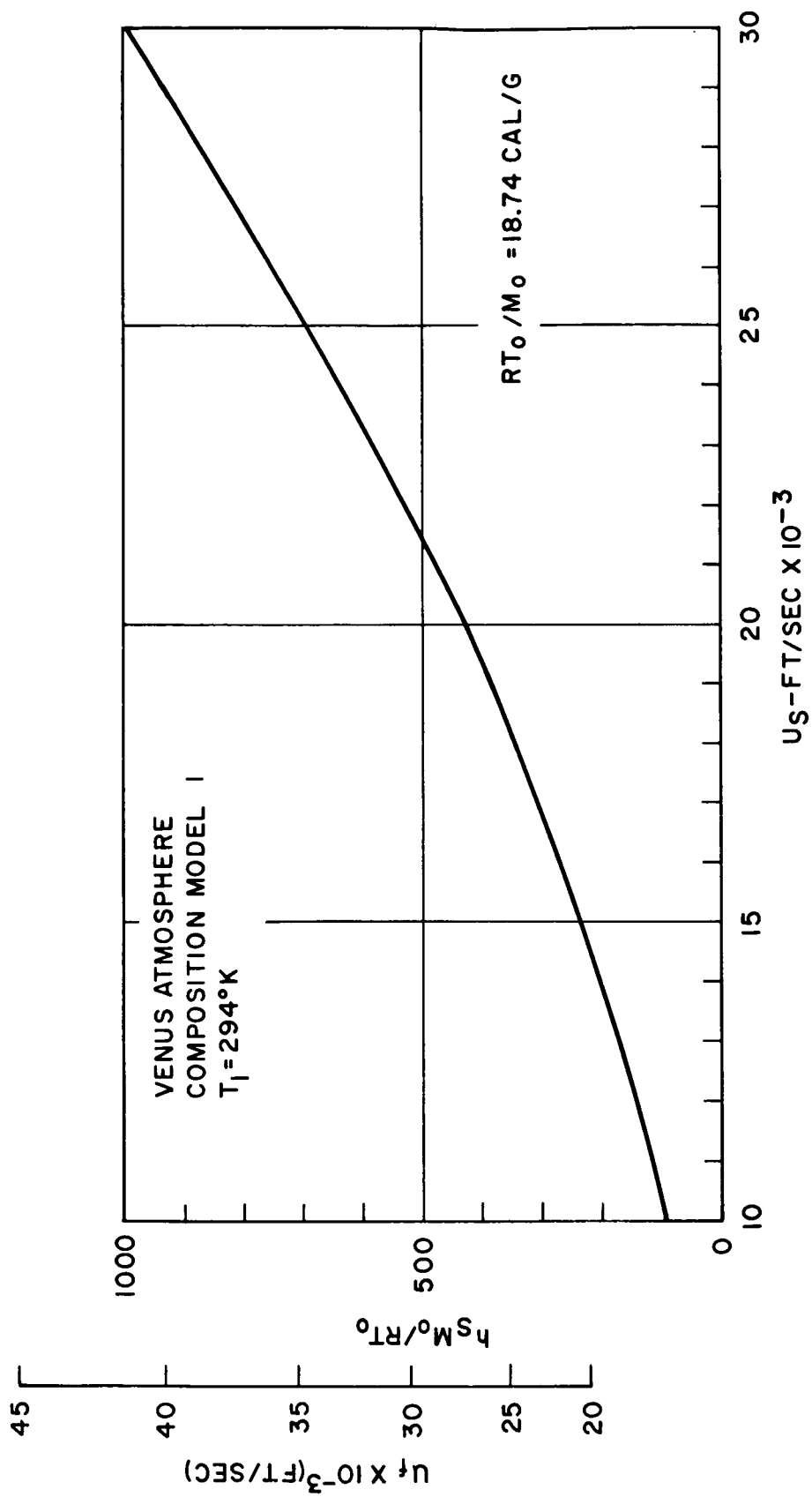
Figure 18.   Stagnation Enthalpy

- 38 -
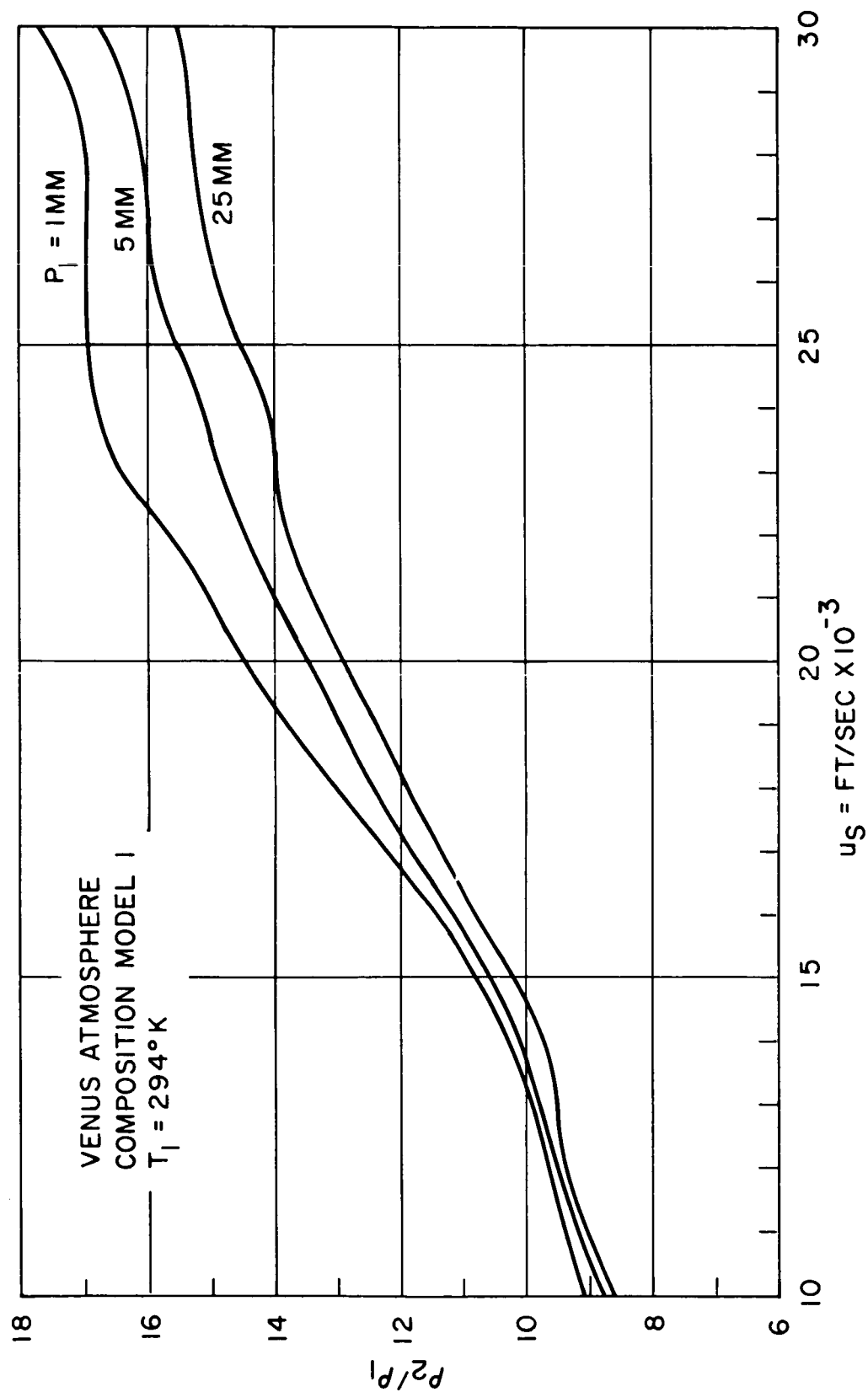
Figure 19.   Density Behind Incident Shock
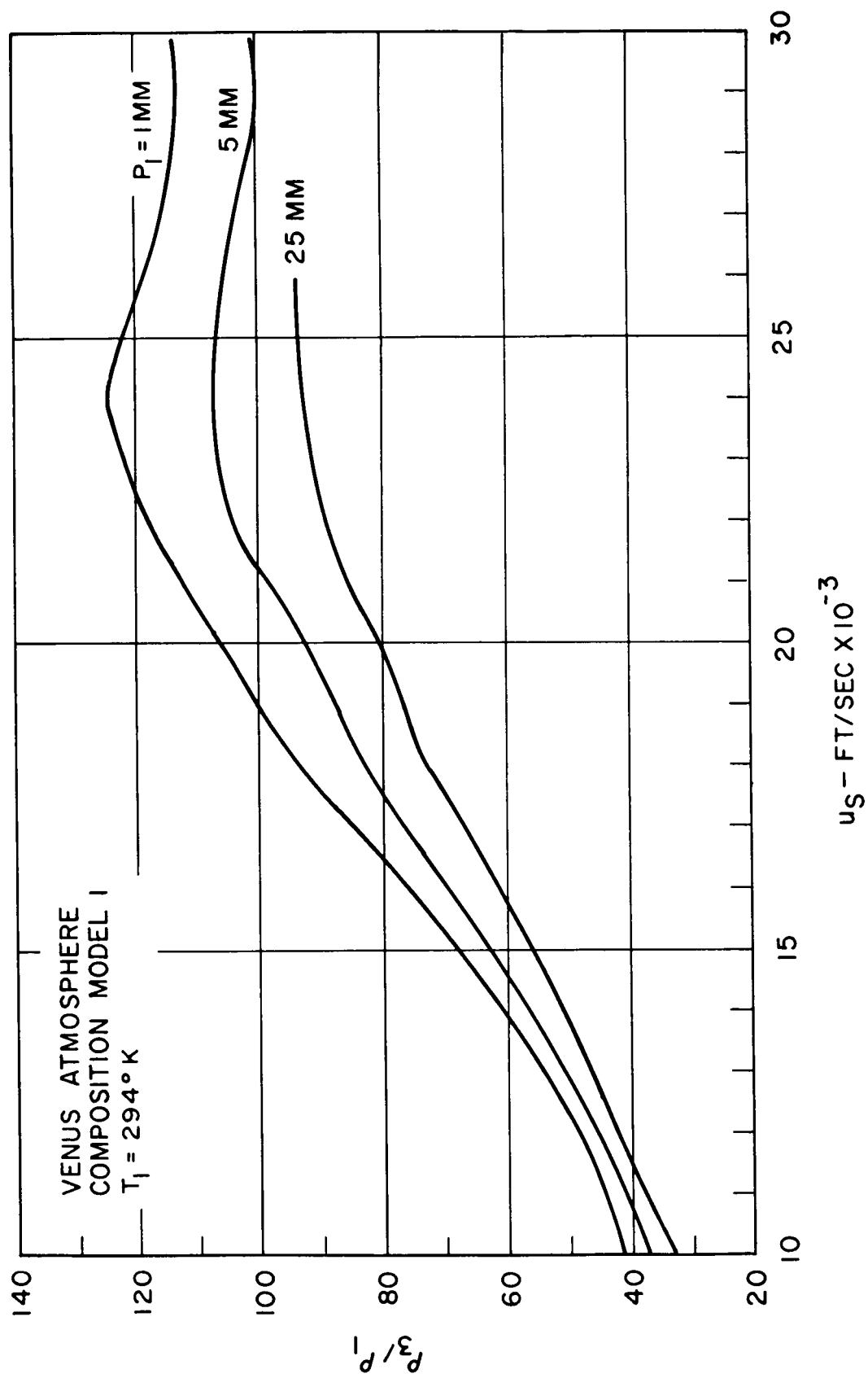
Figure 20 Density Behind Normal Shoc[1]
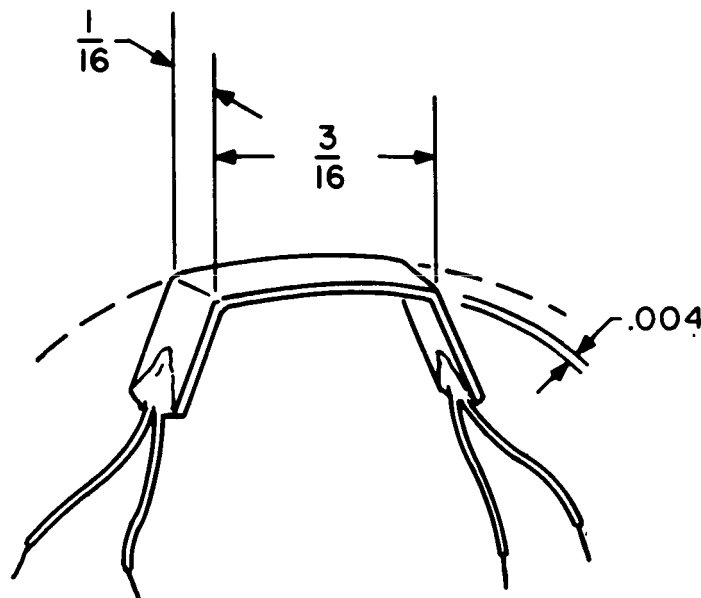
a. CALORIMETER GAUGE
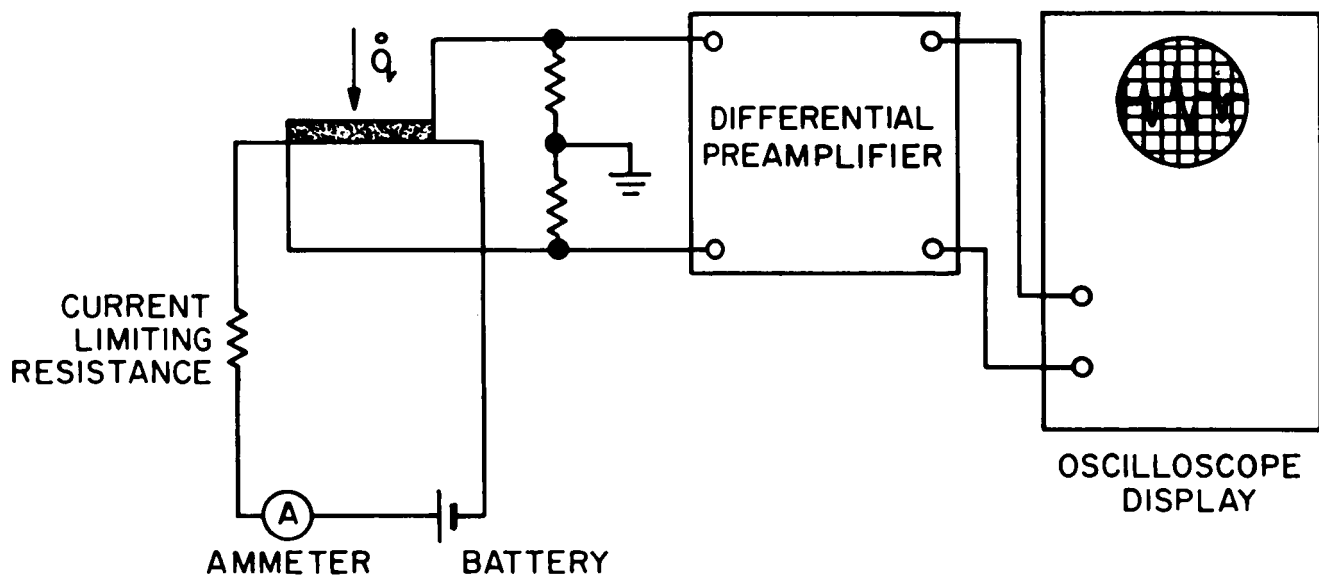
b. SCHEMATIC OF GAUGE CIRCUIT

Figure 7.   Heat Transfer Rate Measurement Set-up.

ADVANTAGES:
1. WINDOWLESS AND NO SURFACE EFFECT UNCERTAINTY. ACCEPTS AND MEASURES ALL INCIDENT RADIATION

2. COLLIMATION ALLOWS MEASUREMENT OF TOTAL EMISSION FROM LOCAL AREAS OF HEATED GAS WITH μs RESOLUTION.
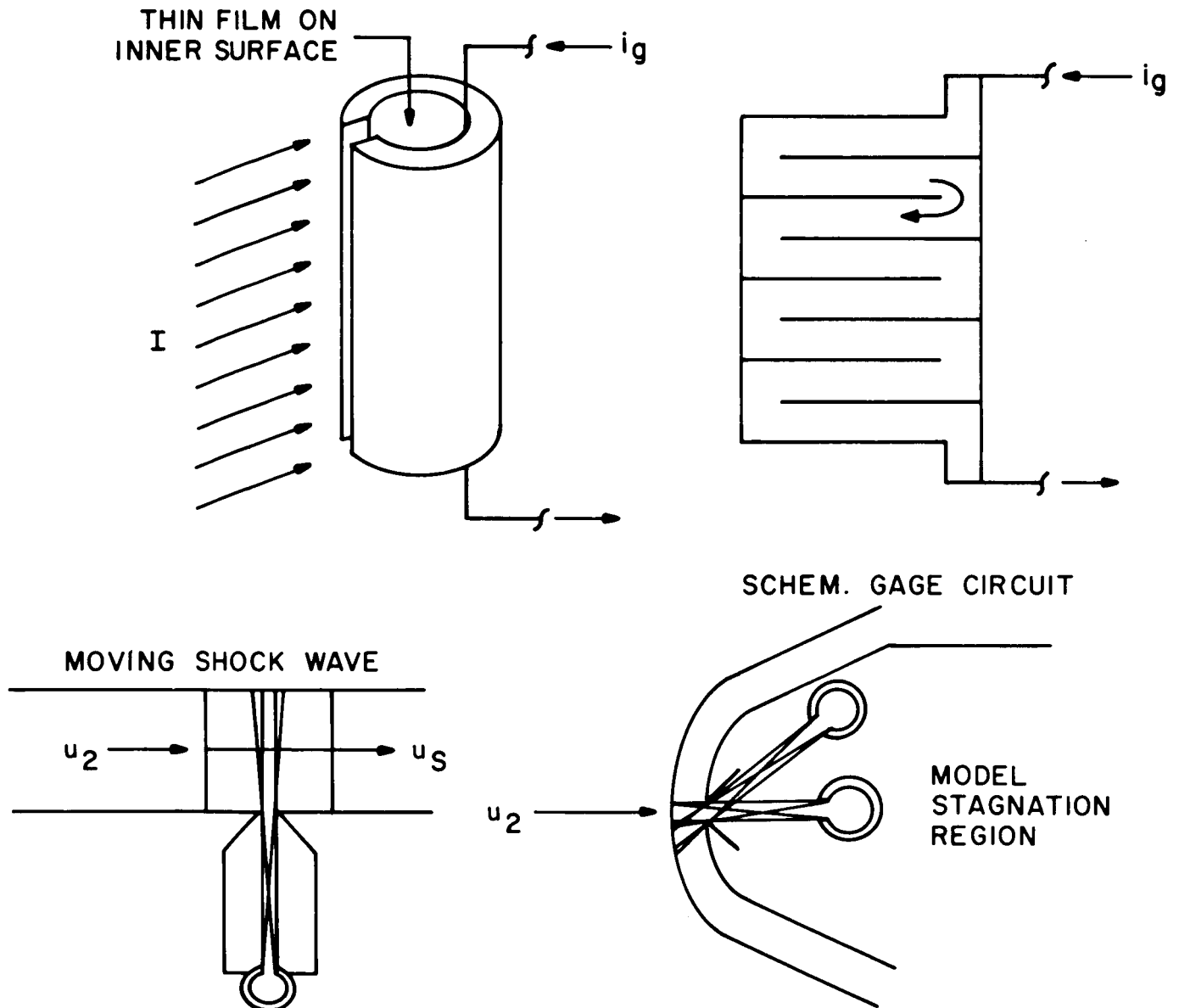
Figure 8.   Cavity Gage for Total Radiative Heat Transfer Measurements
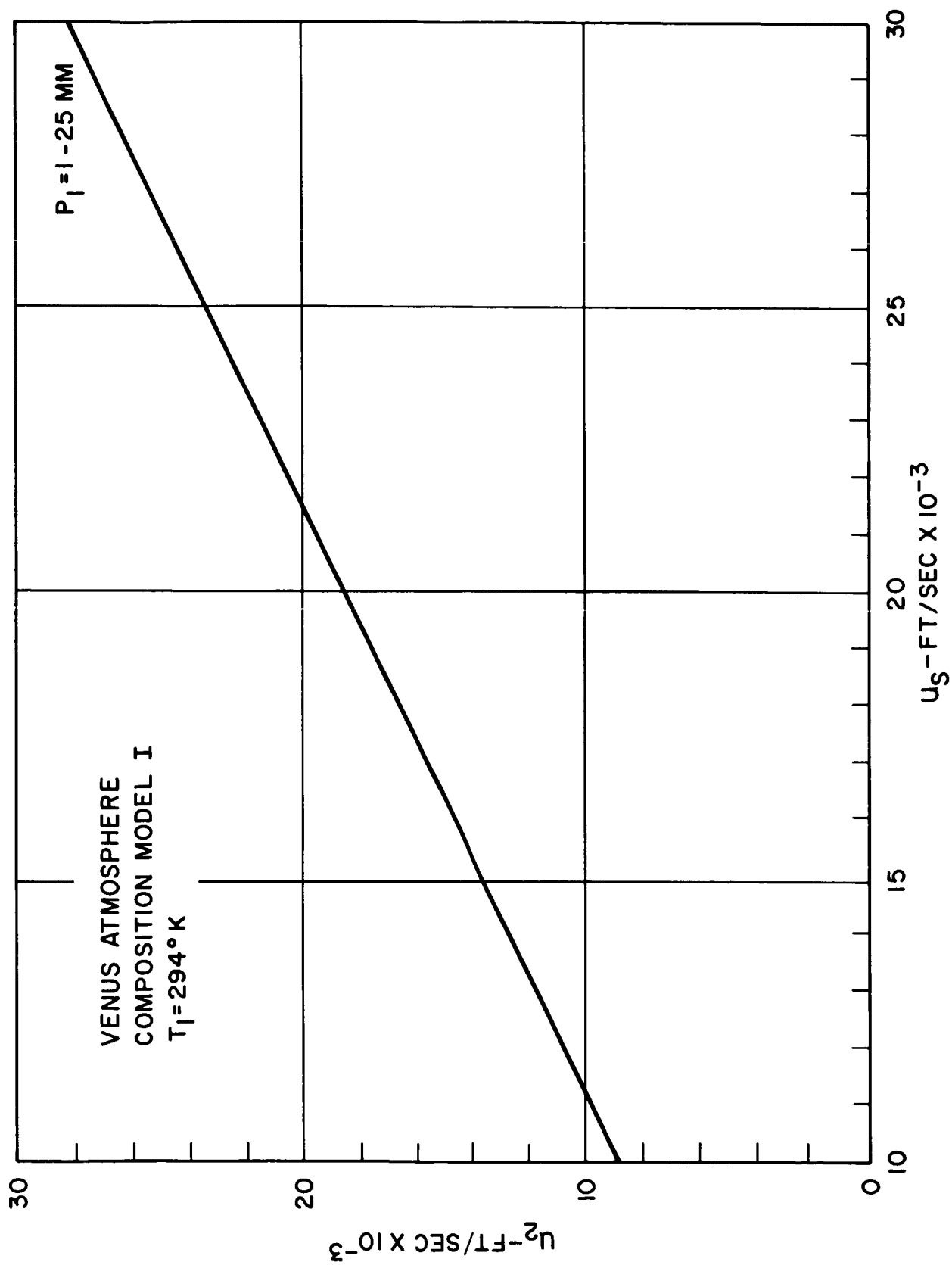
Figure 21. Velocity Behind Incident Shock
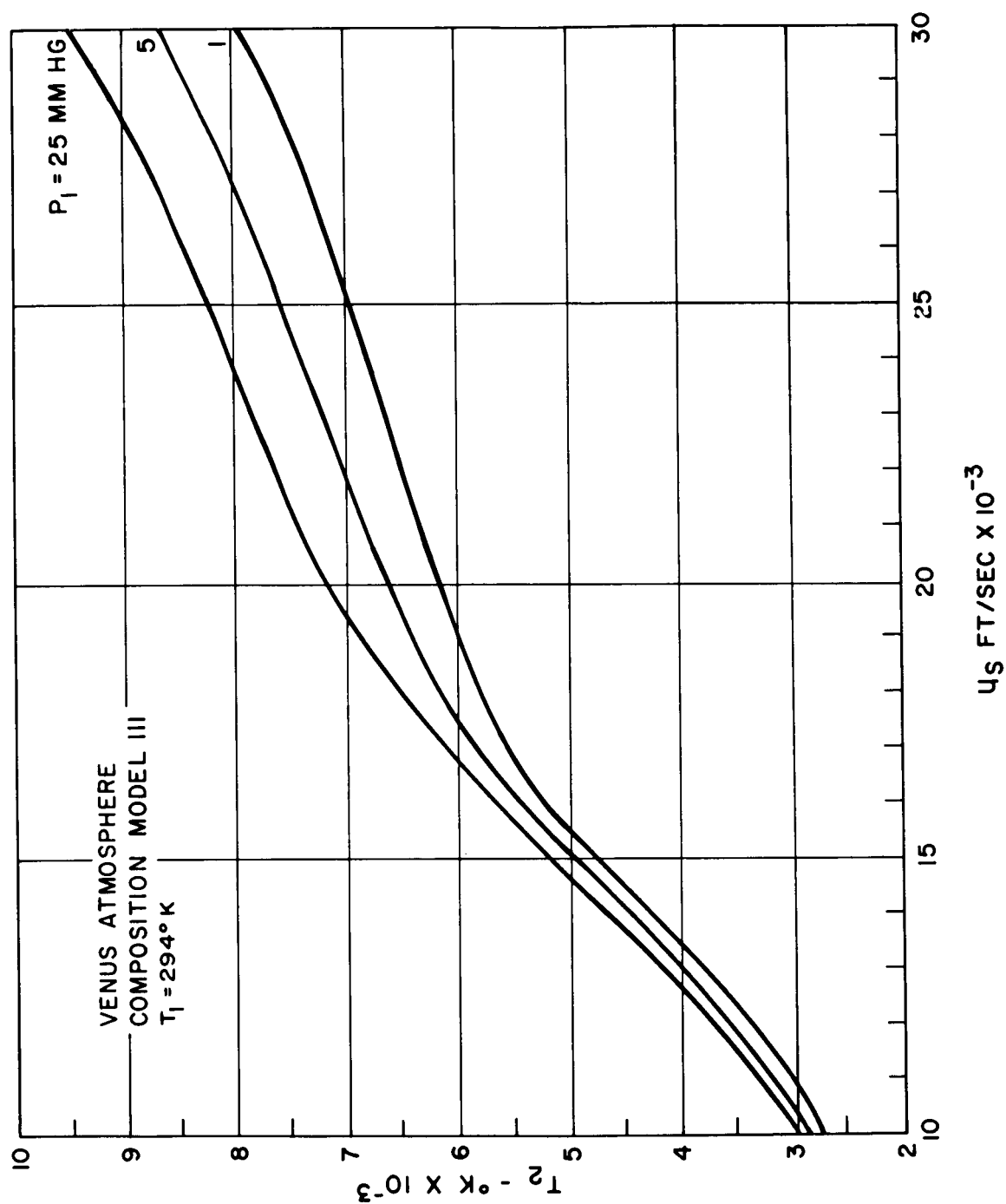
Figure 22.   Temperature Behind Incident Shock
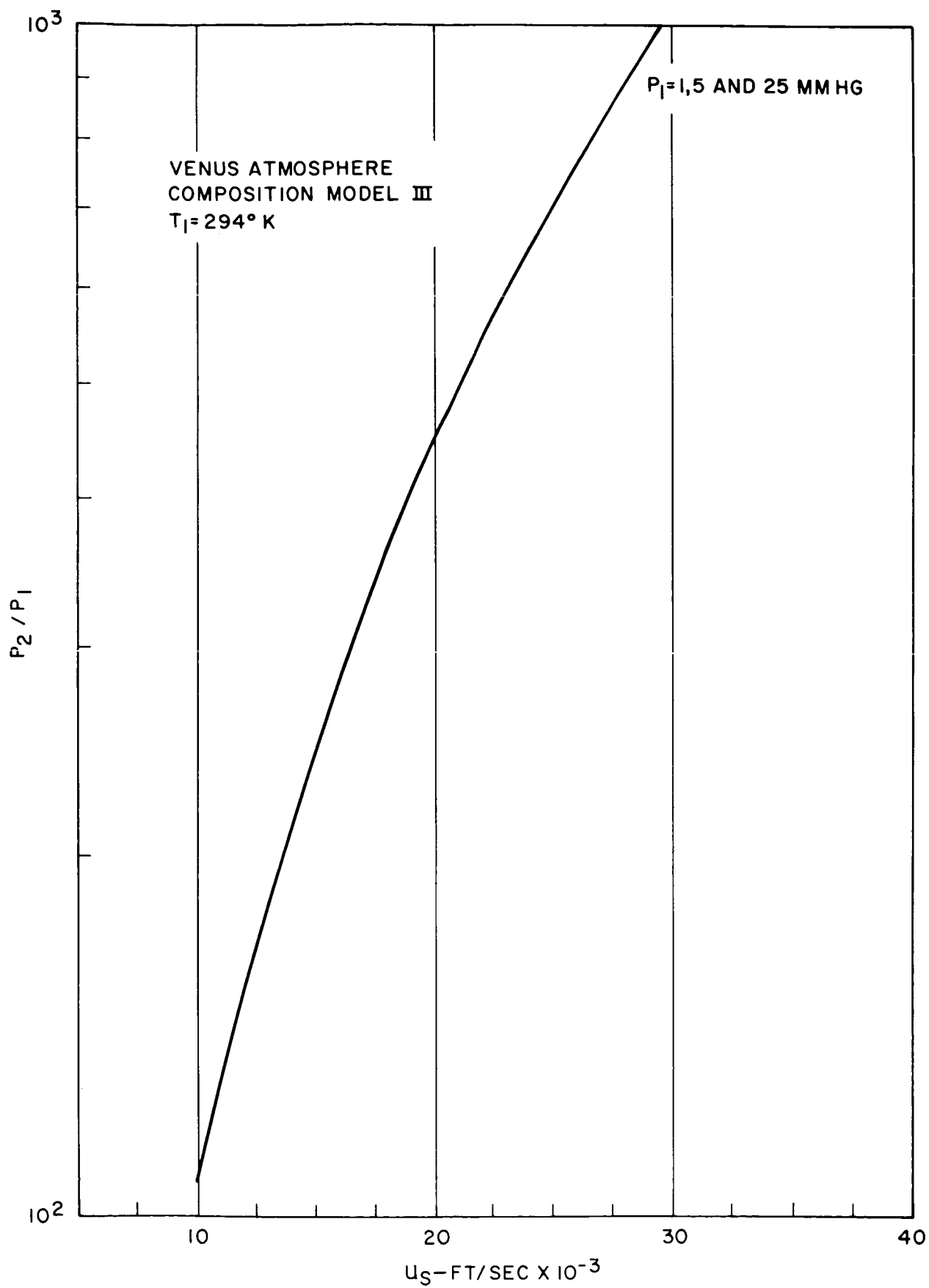
Figure 25.   Pressure Behind Incident Shock
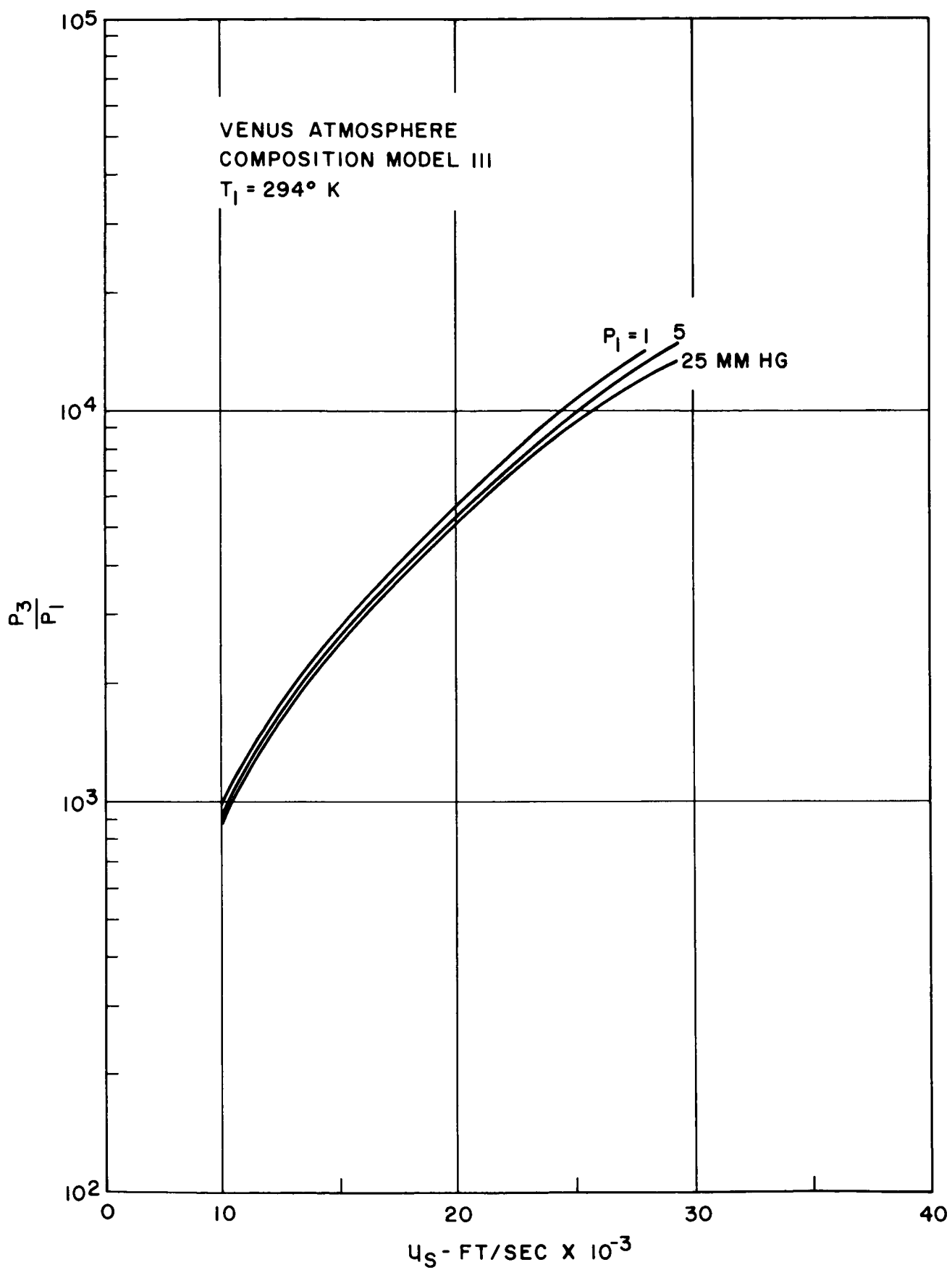
Figure 26. Pressure Behind Normal Shock
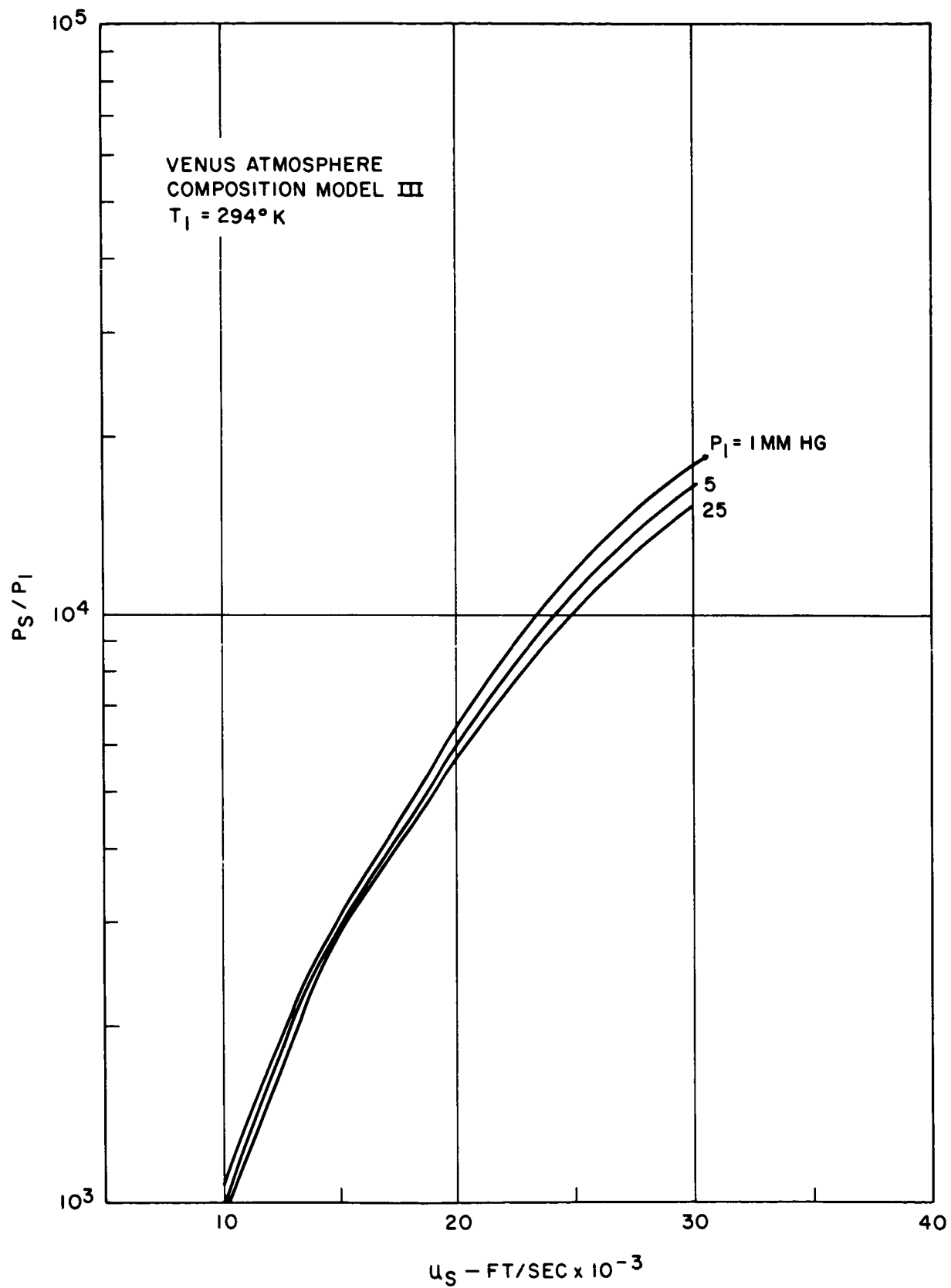
Figure 27. Stagnation Pressure

- 47 -
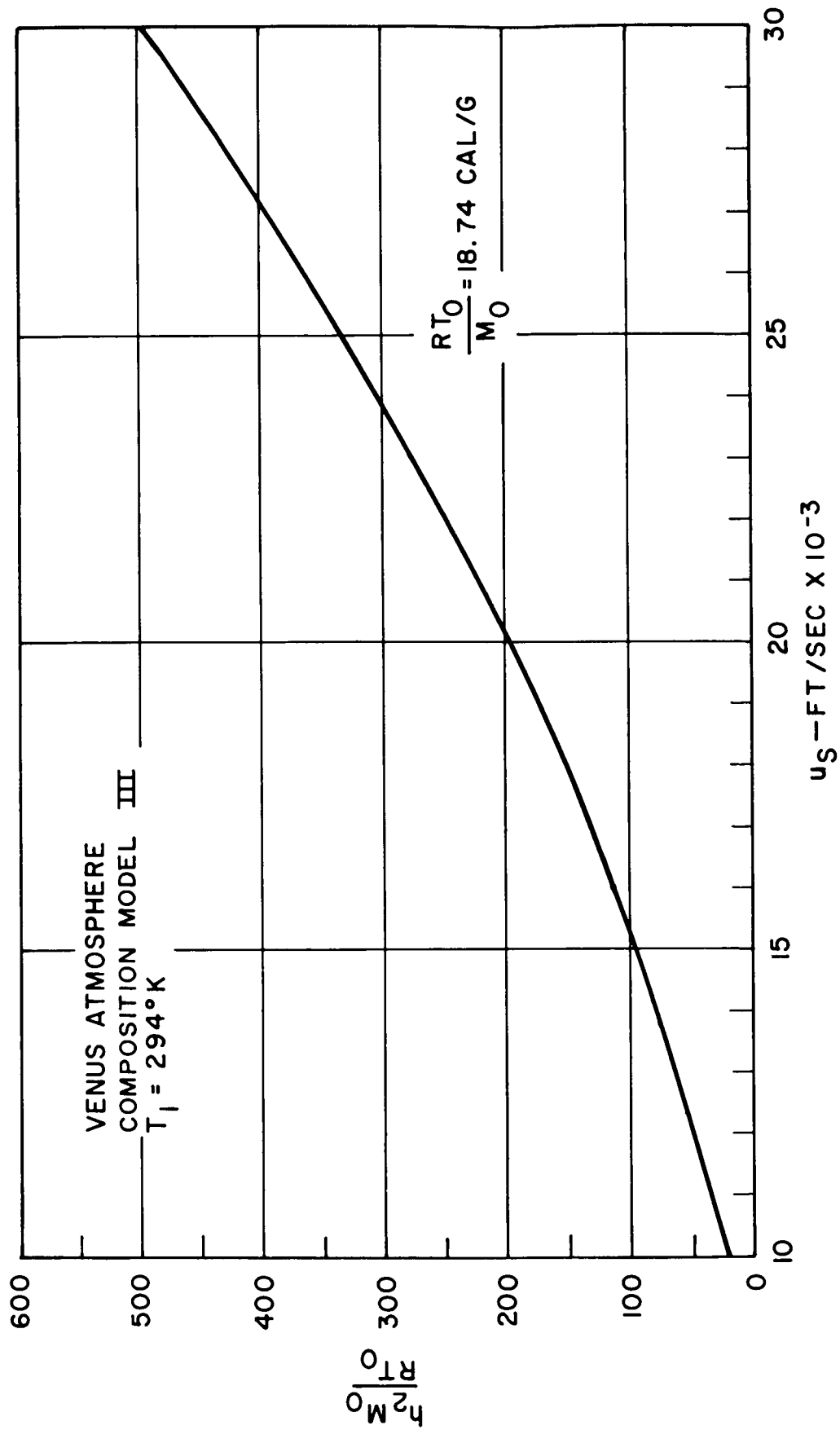
Figure 28. Enthalpy Behind Incident Shock
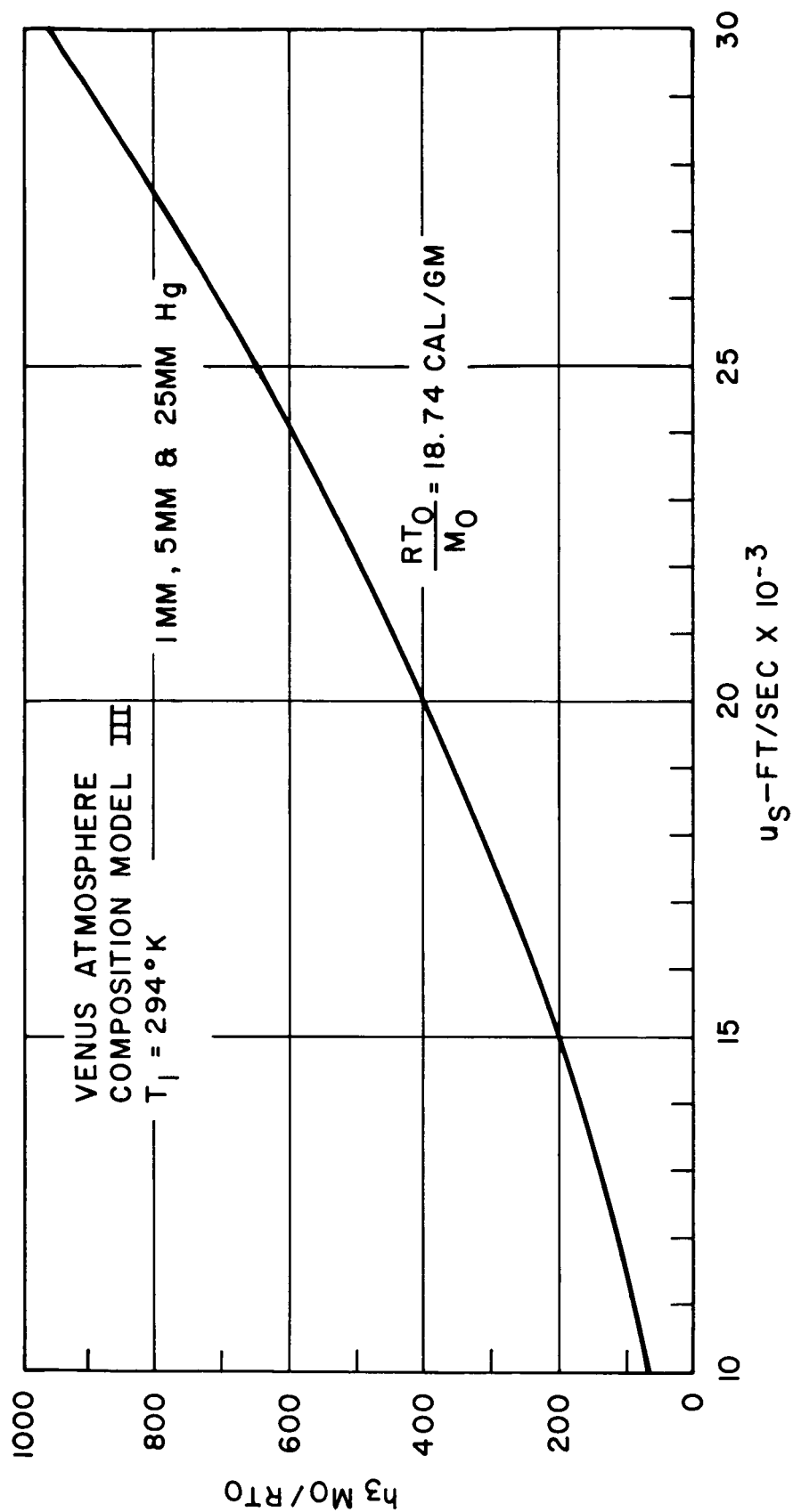
Figure 29. Enthalpy Behind Normal Shock
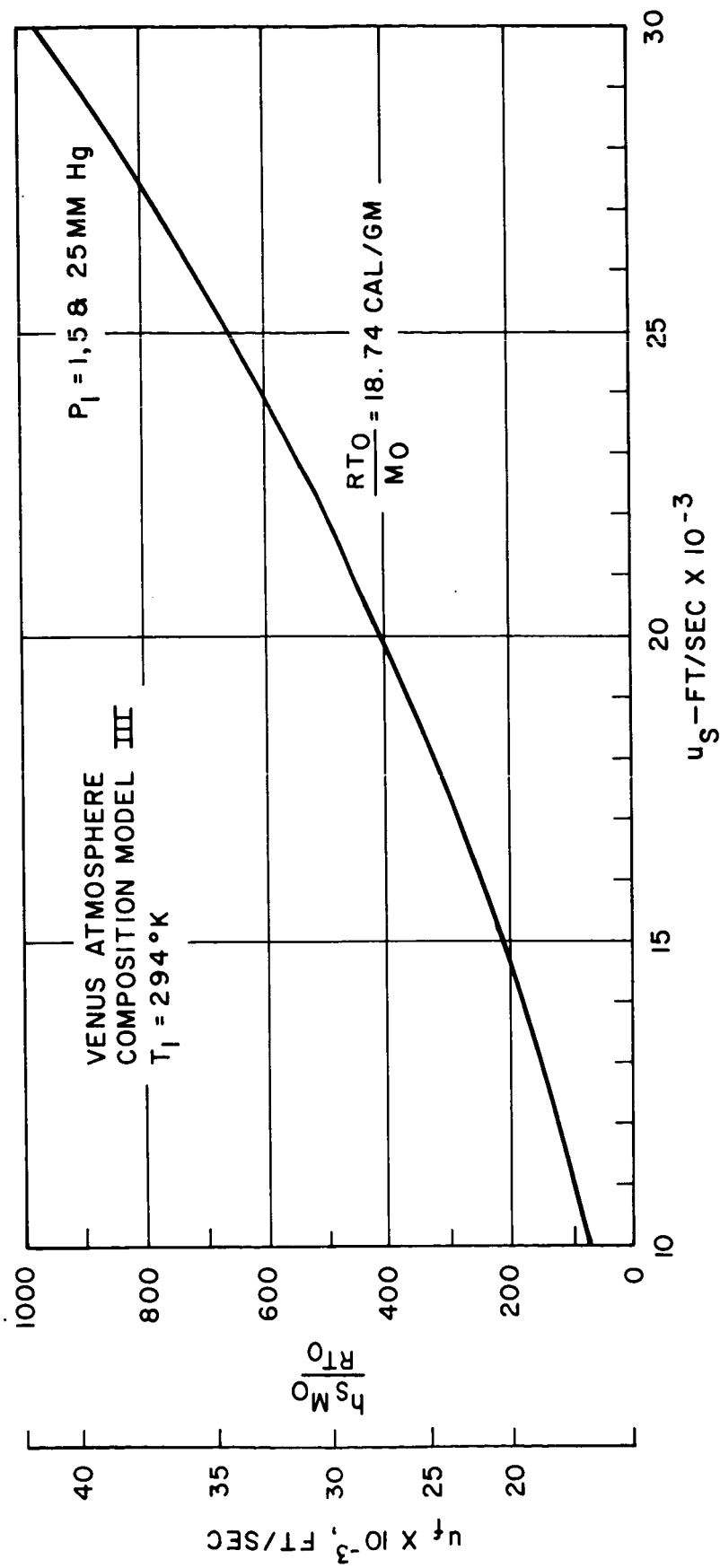
Figure 30. Stagnation Enthalpy
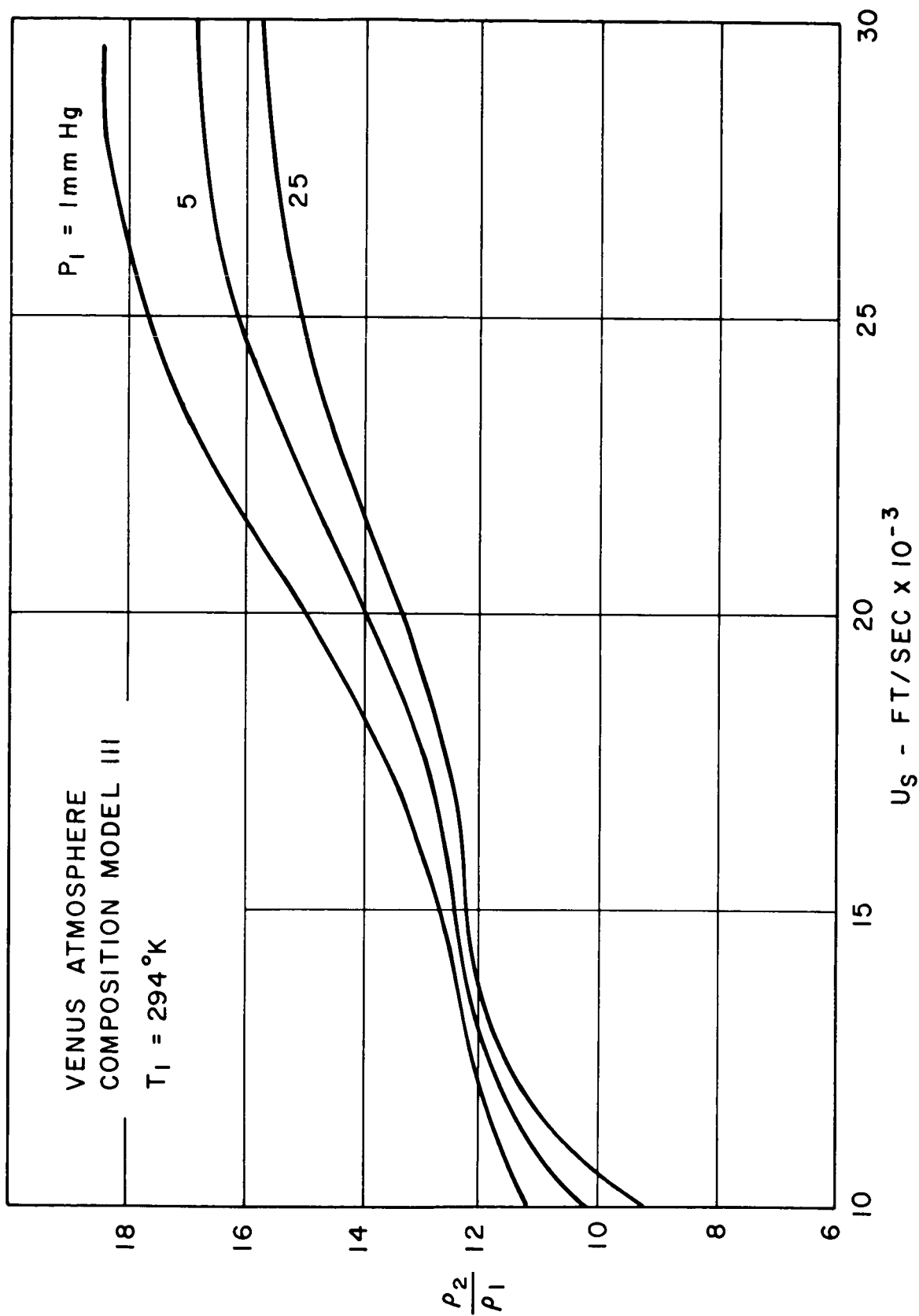
Figure 31. Density Behind Incident Shock
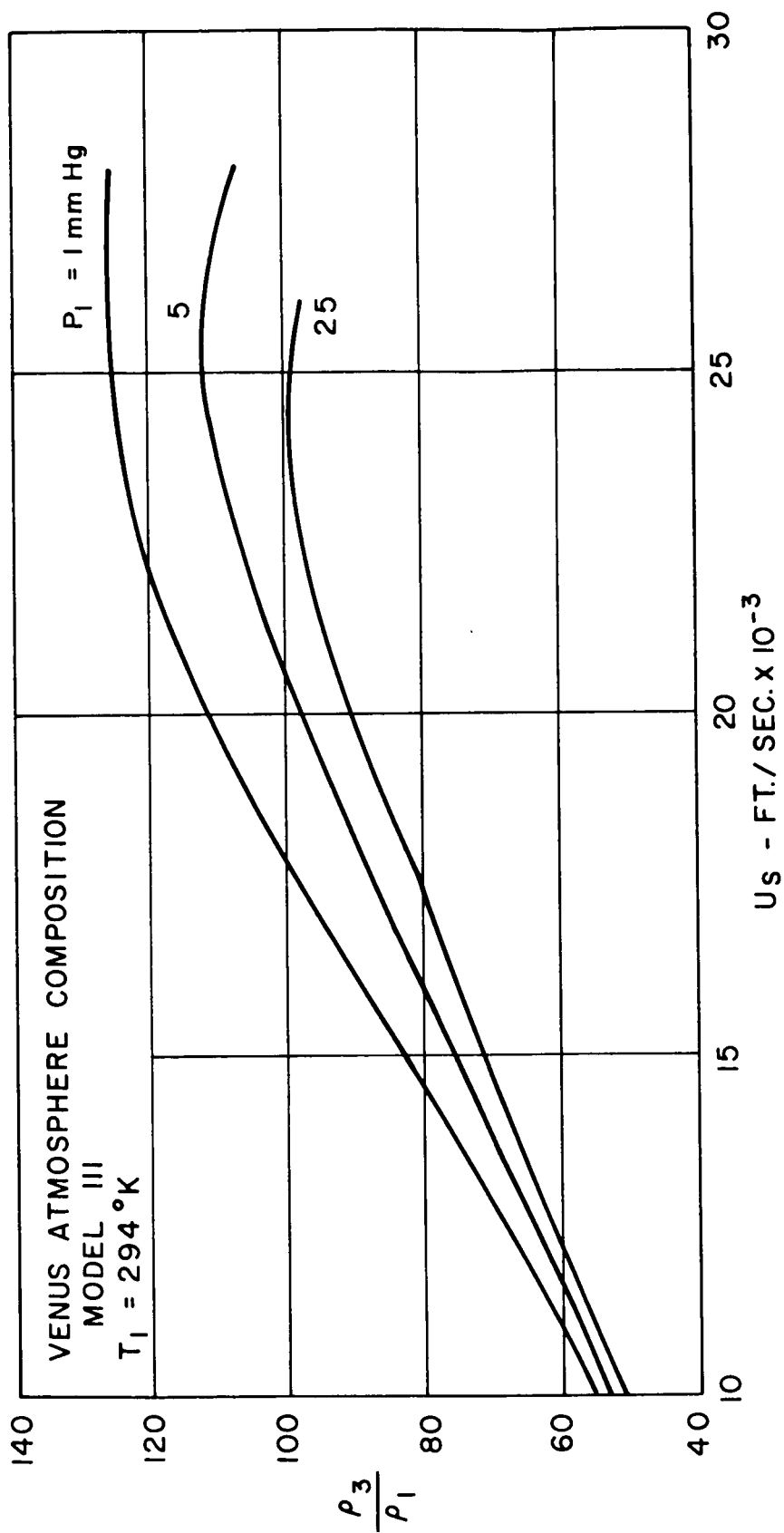
Figure 32. Density Behind Normal Shock
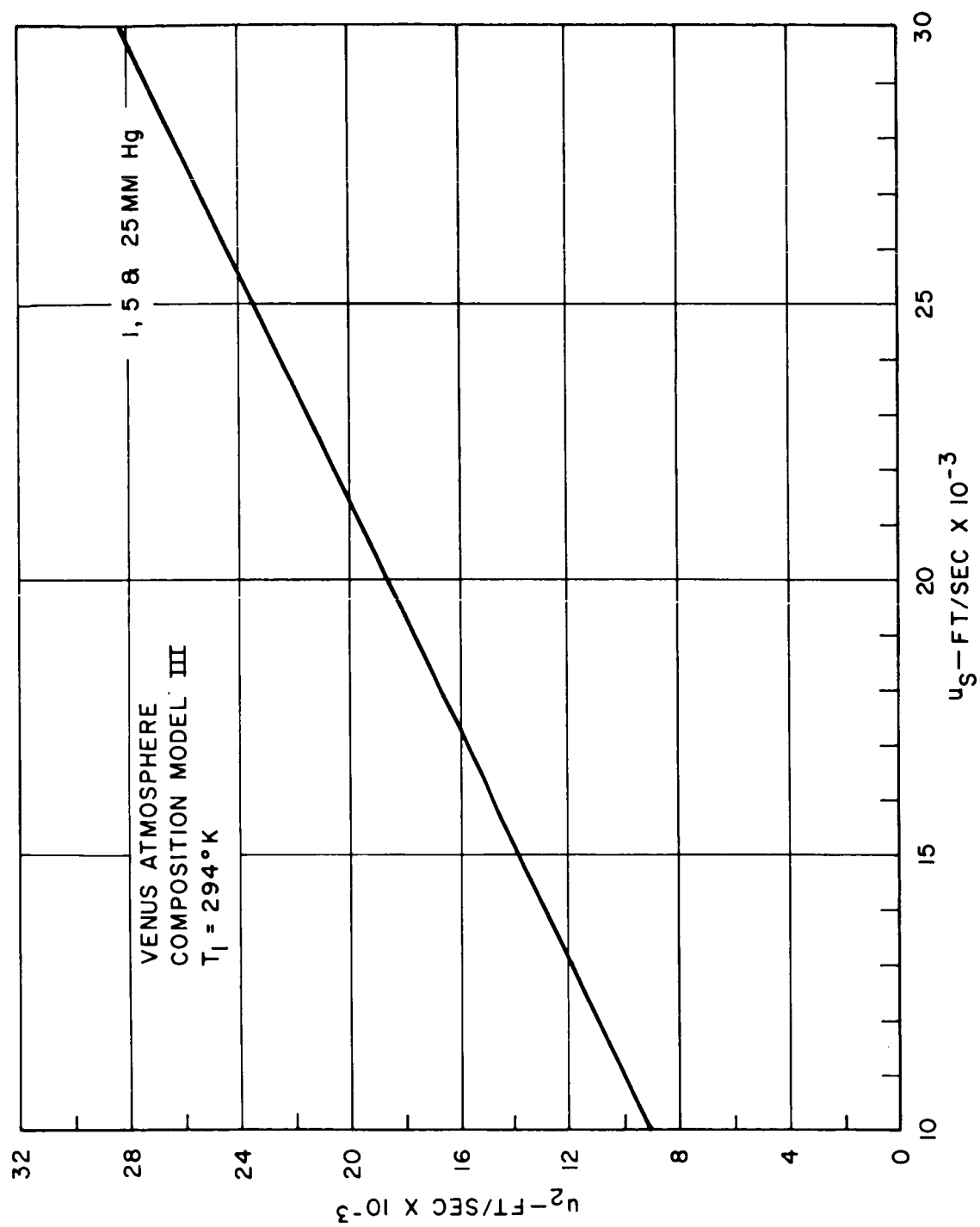
Figure 33. Velocity Behind Incident Shock
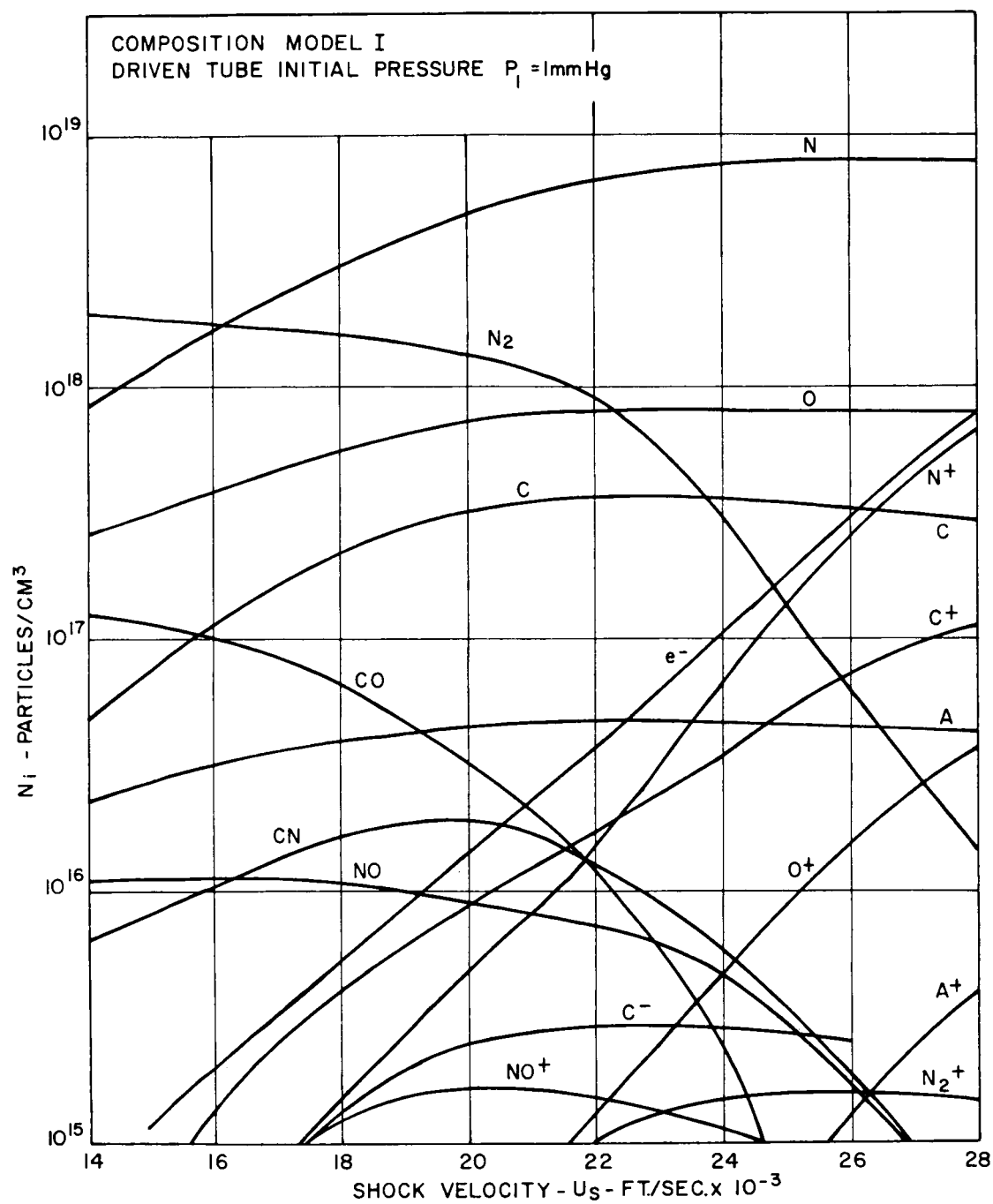
Figure 34. Equilibrium Composition of Venus Atmosphere at Stagnation

Point of a Hemispherical Model
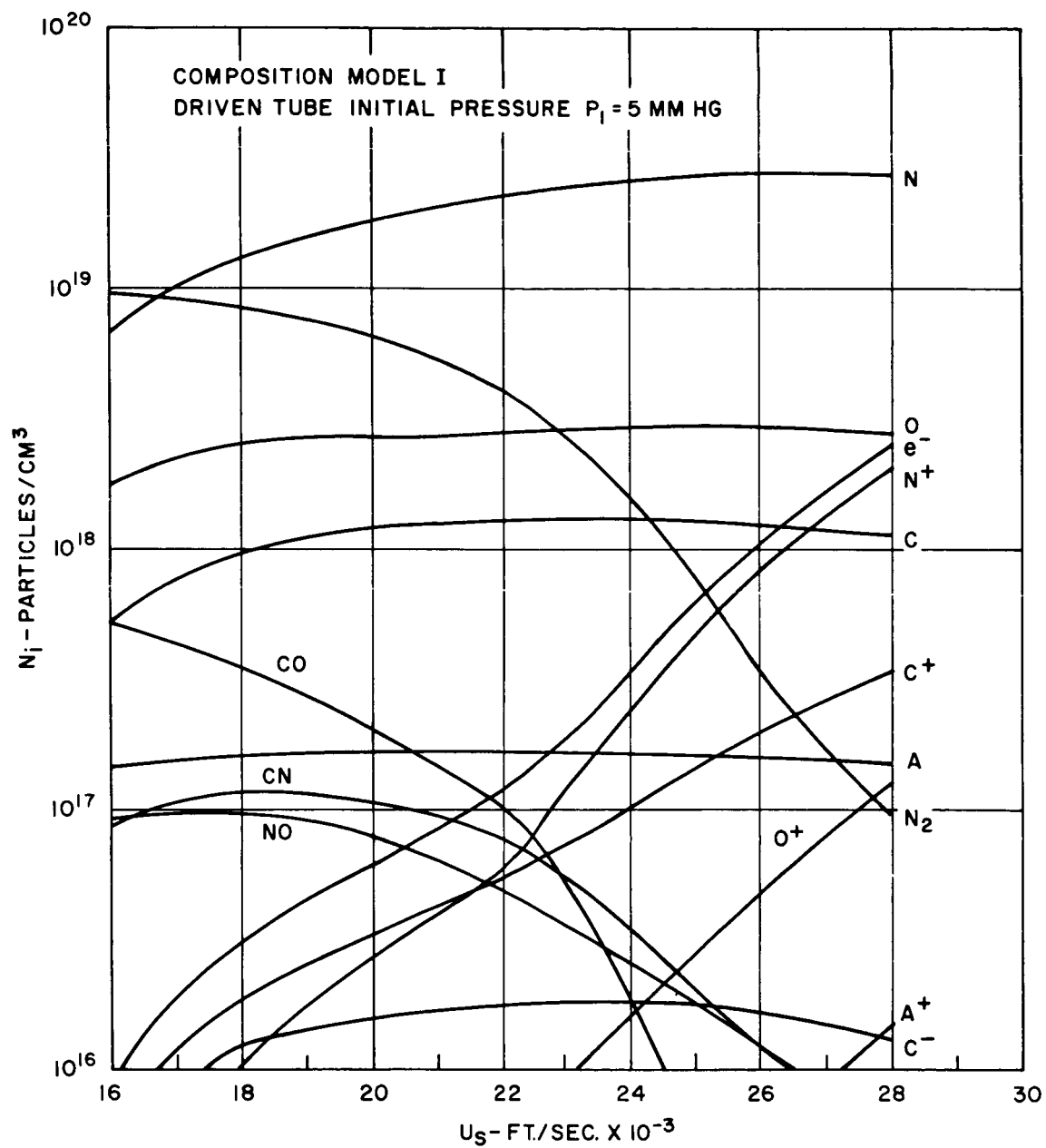
Figure 35. Equilibrium Composition of Venus Atmosphere at Stagnation
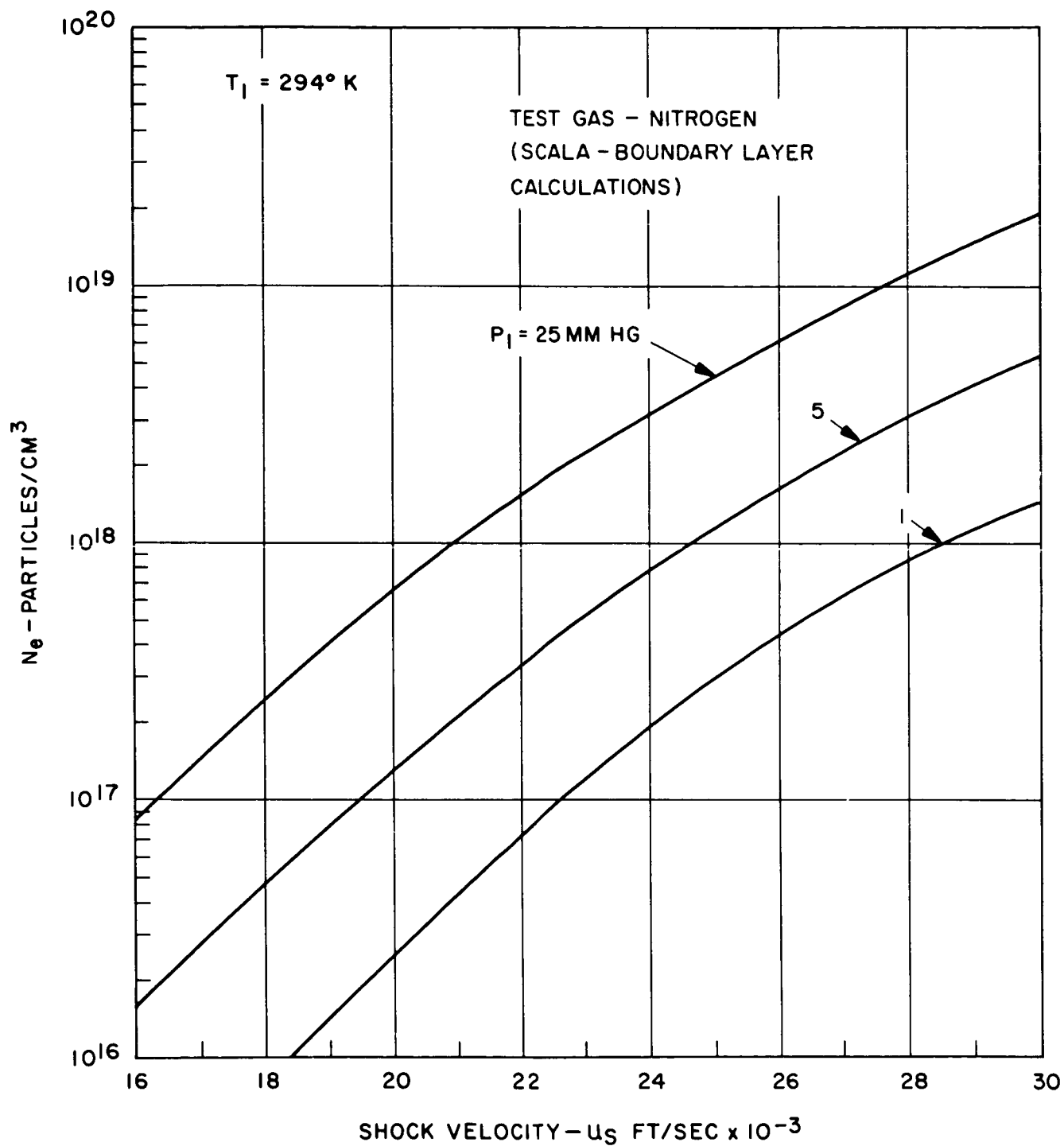Point of a Hemispherical Model
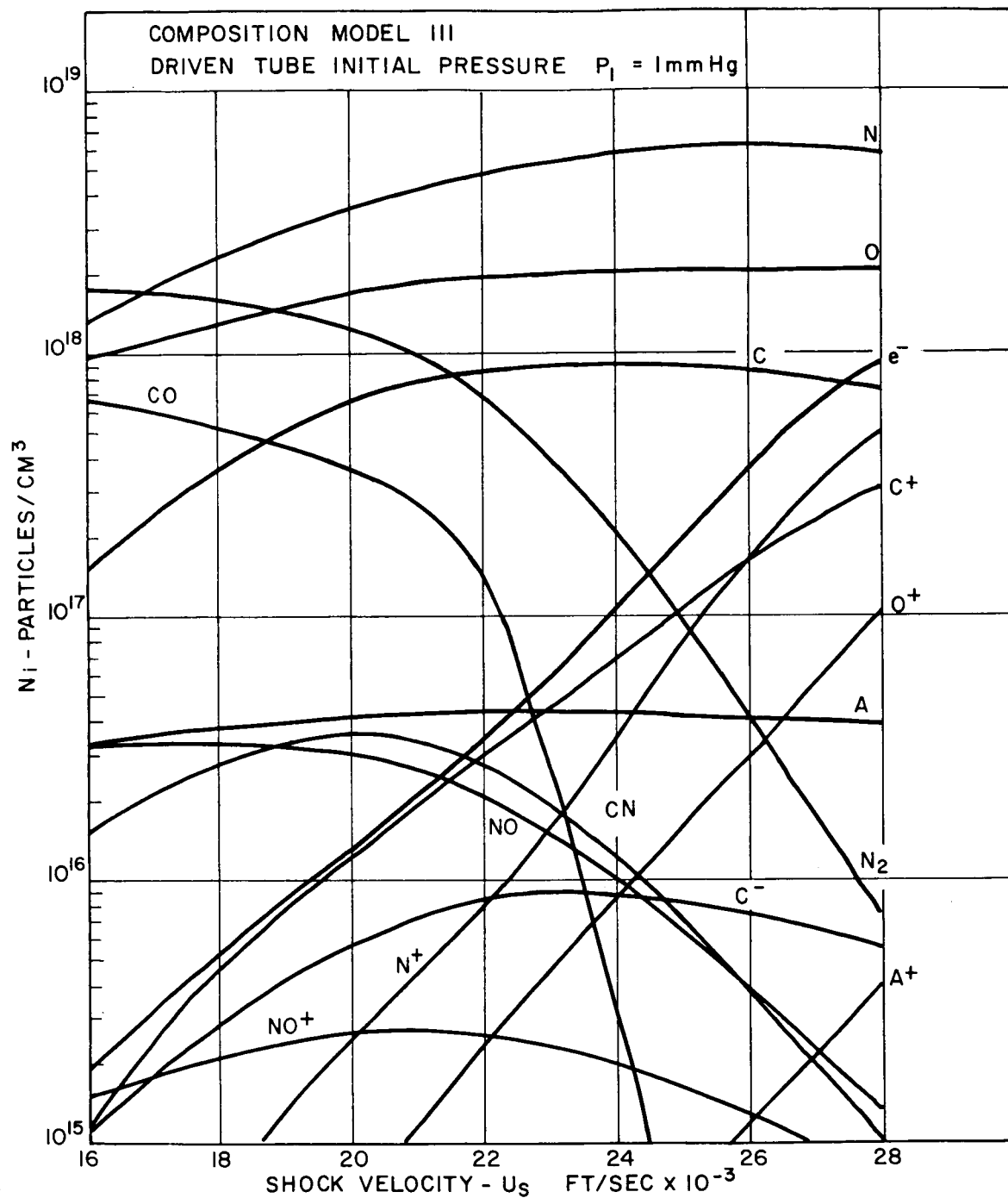
Figure 36. Equilibrium Composition of Venus Atmosphere at Stagnation
Point of a Hemispherical Model
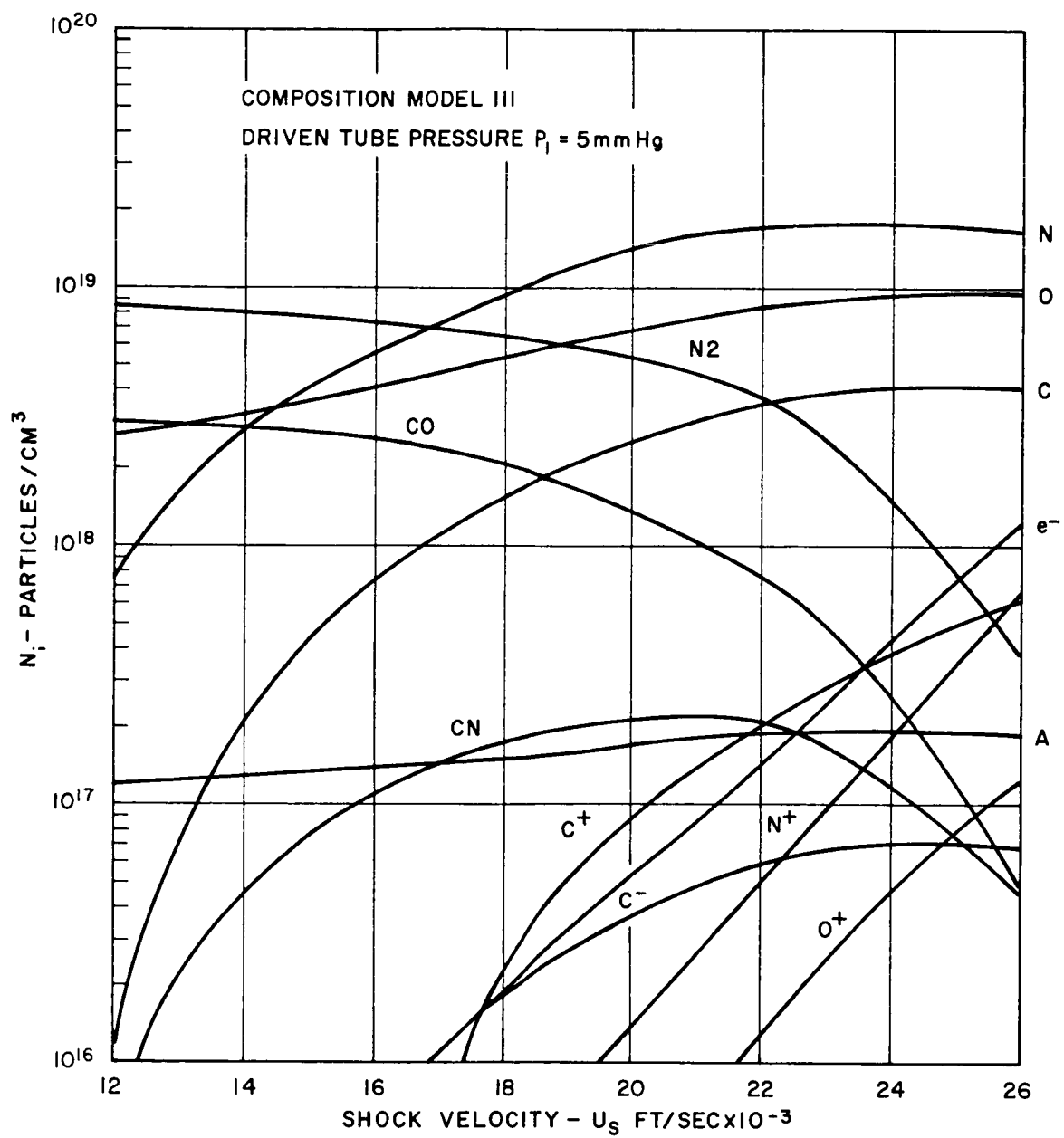
Figure 37. Equilibrium Composition of Venus Atmosphere at Stagnation Point of a Hemispherical Model
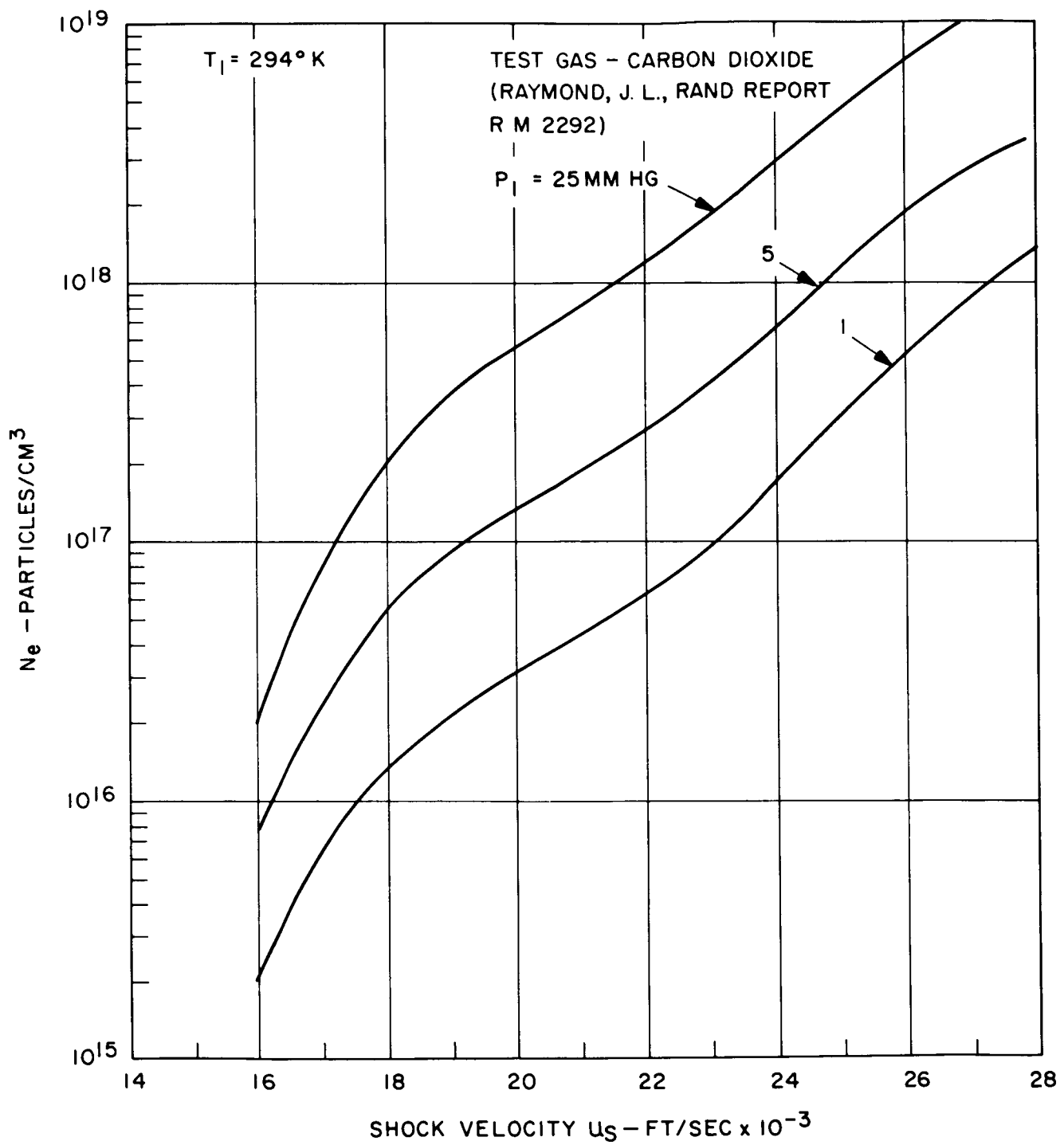
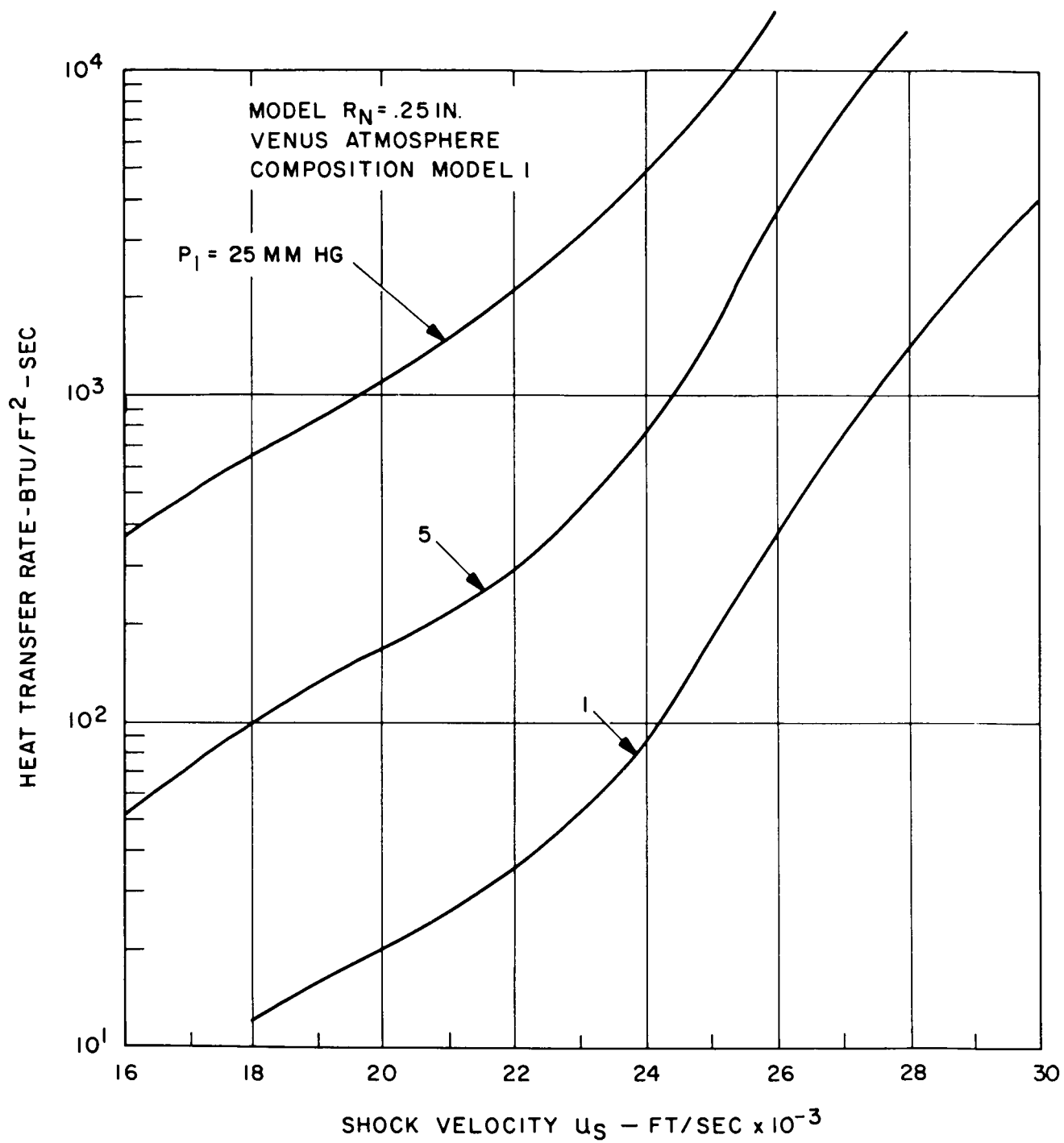Figure 38. Equilibrium Concentration of Electrons at the Stagnation Point of a Hemispherical Model

Figure 39. Equilibrium Concentration of Electrons at the Stagnation

Point of a Hemispherical Model

Figure 40. Equilibrium Radiative Heat Transfer to the Stagnation Point
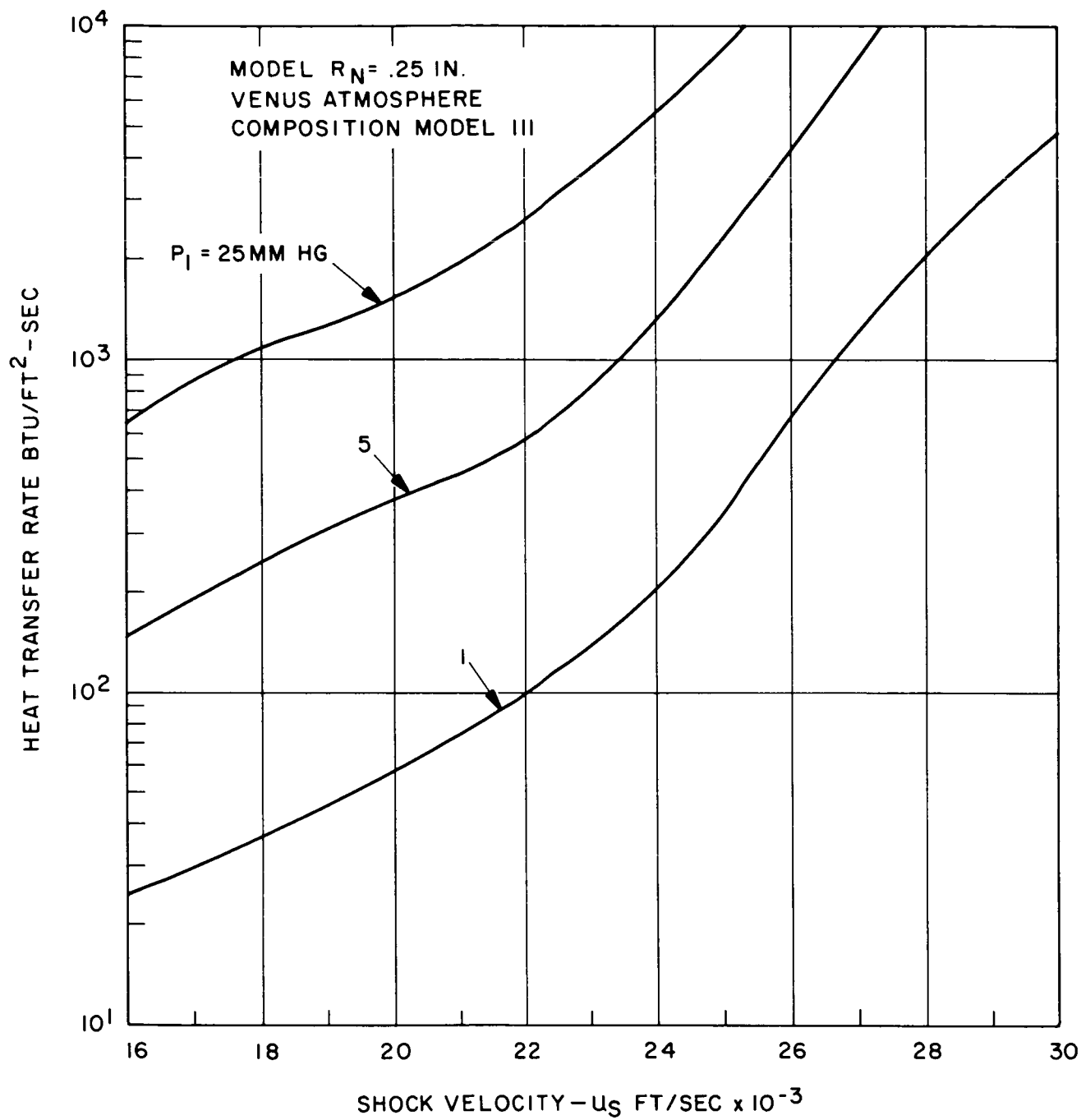
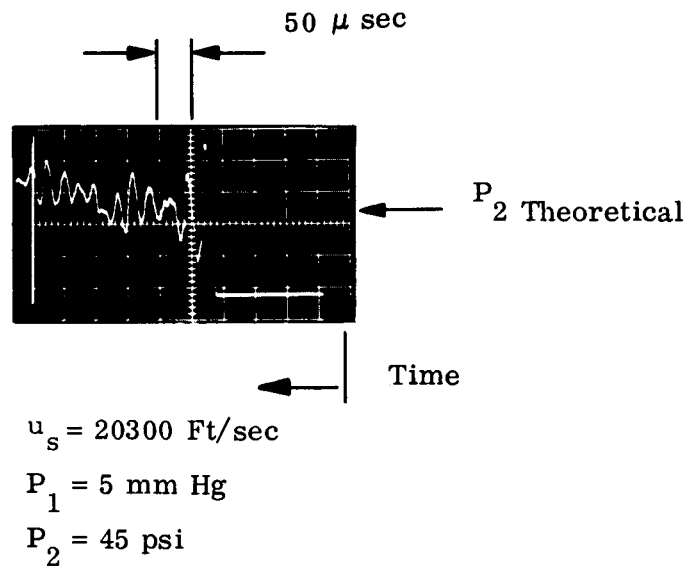Figure 41. Equilibrium Radiative Heat Transfer to the Stagnation Point

50 μ sec

P_2 Theoretical

Time

u_s = 20300 Ft/sec

P_1 = 5 mm Hg

P_2 = 45 psi

Figure 42. Typical Oscillogram of Pressure Behind Incident Shock (Signal Unfiltered)

10 μ sec

5 μ sec Shock Arrival

Time

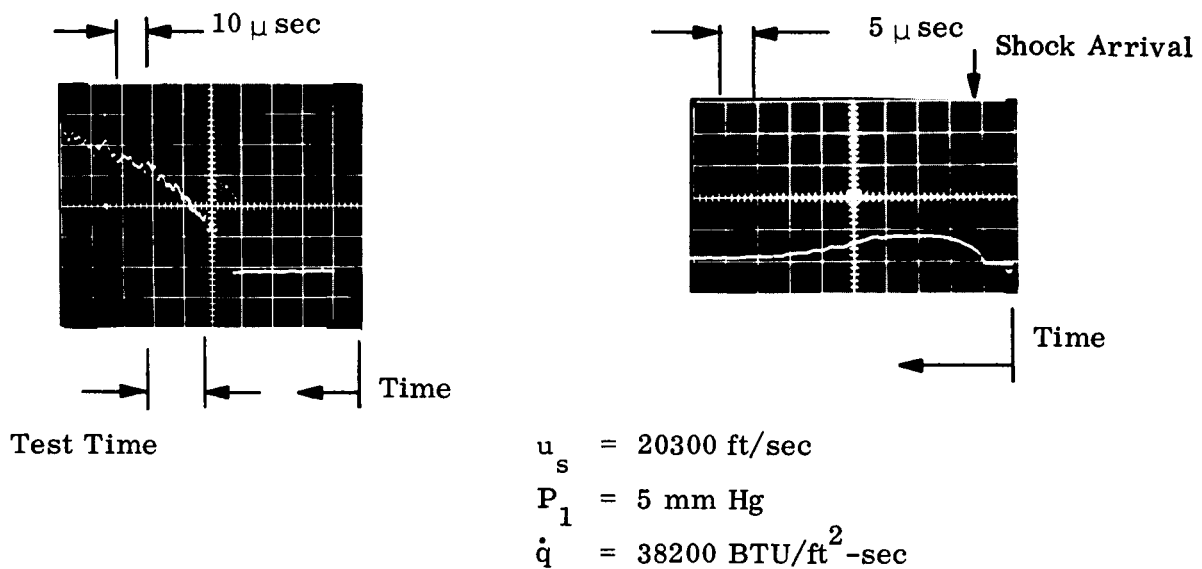Test Time

Time

u_s = 20300 ft/sec

P_1 = 5 mm Hg

$\dot{q}$ = 38200 BTU/ft^2-sec

Figure 43. Typical Oscillograms from Heat Transfer Gage and Corresponding Pyrometer Signal of Incident Shock Wave

Shock Arrival

u_s = 29200 ft/sec
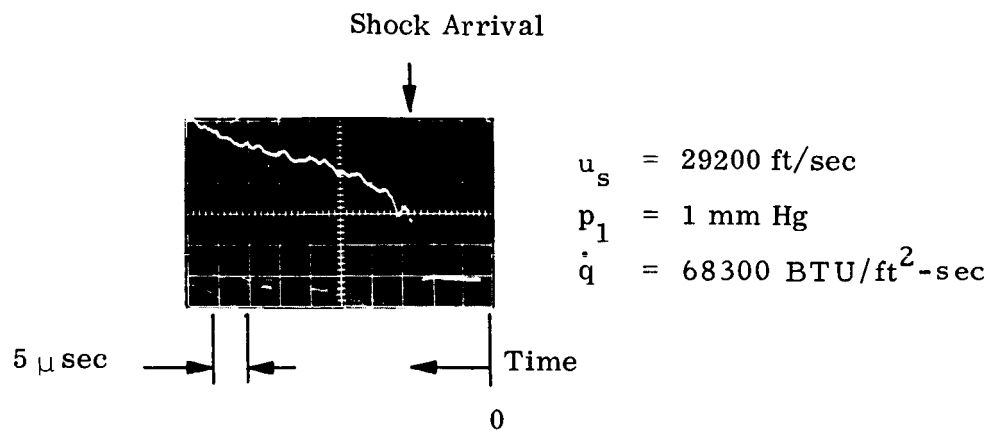
p_1 = 1 mm Hg

$\dot{q}$ = 68300 BTU/ft^2-sec

5 μ sec ⟶ Time

0

Figure 44. a   Typical Oscillogram From Hytemco Calorimeter

Heat Transfer Gage

Shock Arrival

u_s = 29600 ft/sec

p_1 = 1 mm Hg
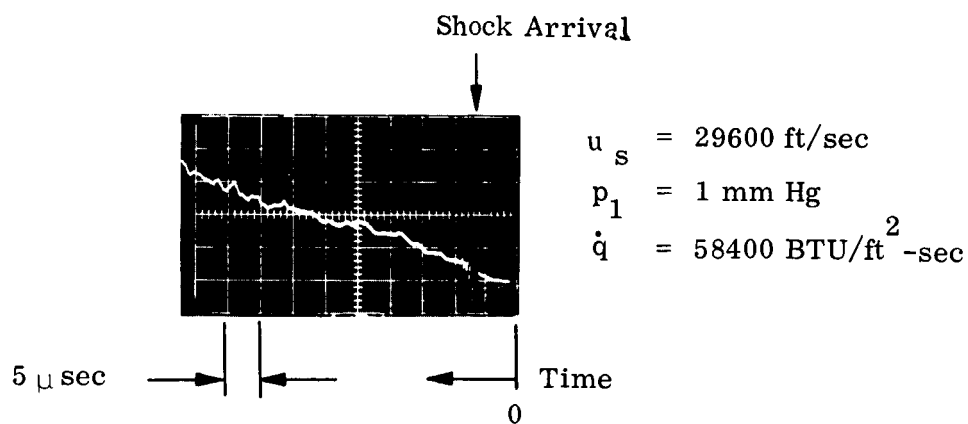
$\dot{q}$ = 58400 BTU/ft^2-sec

5 μ sec ⟶ Time

0

Figure 44. b. Typical Oscillogram from Platinum Calorimeter Heat
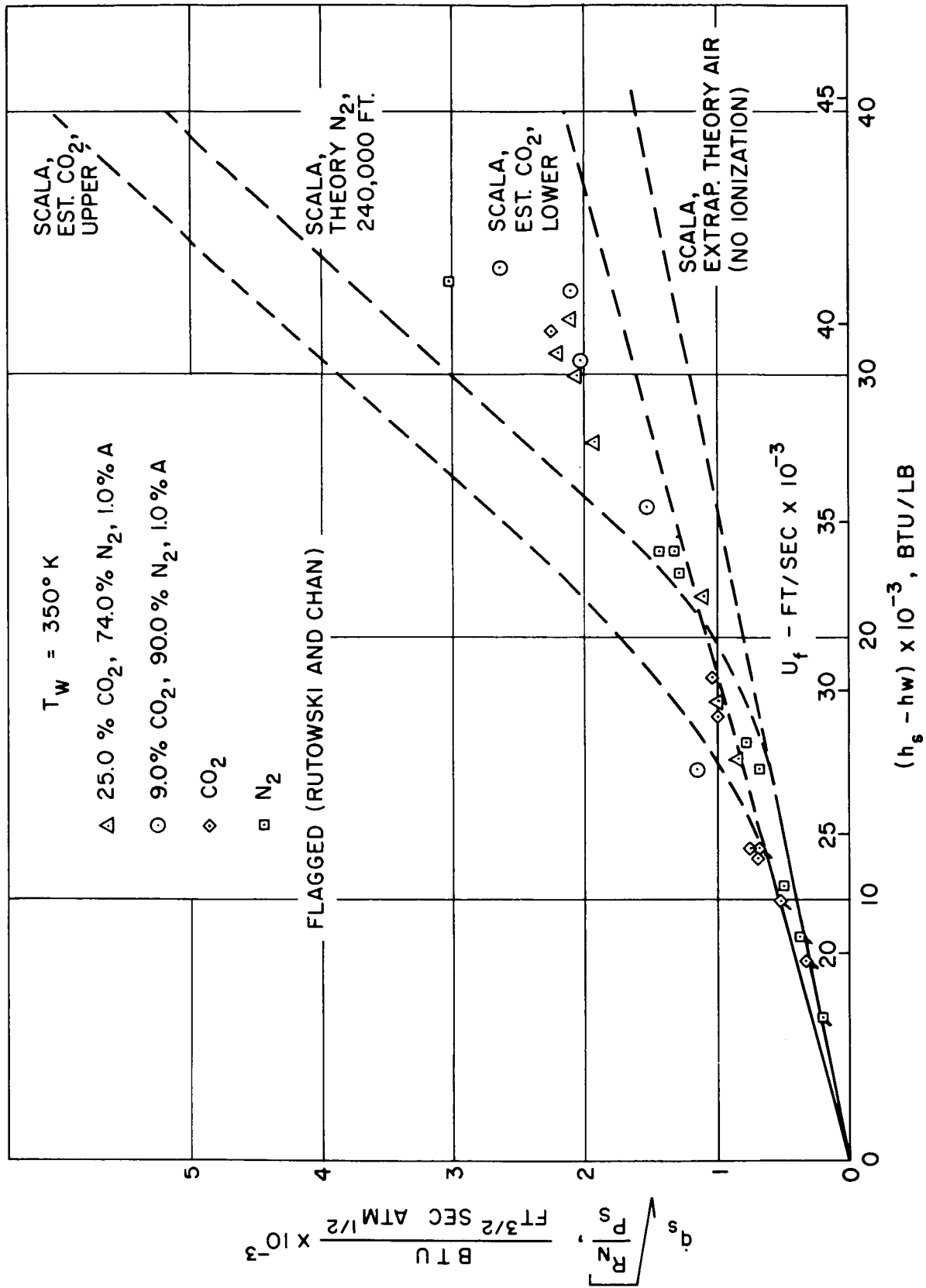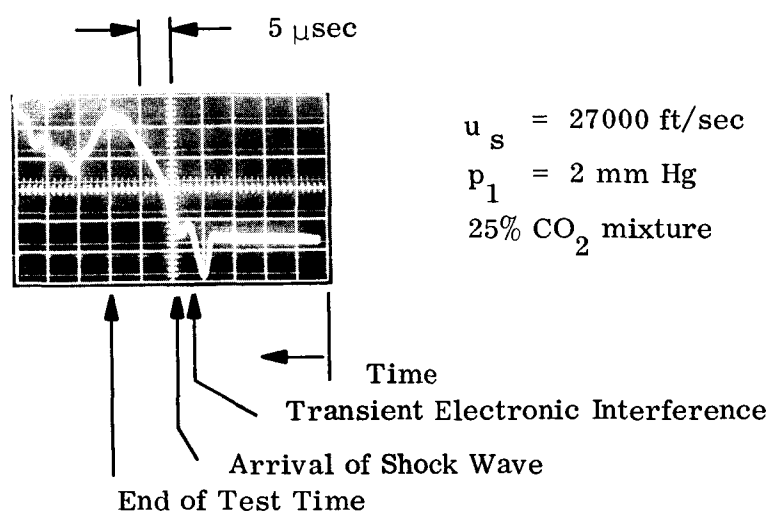
Transfer Gage

Figure 45. Stagnation Heat Transfer

Figure 46. Total Radiation Thin Film Cavity Gage Response